Fusion - evaporation reactions in the 7Li+96Zr system

Lukanović, Irena

Master's thesis / Diplomski rad

2019

Degree Grantor / Ustanova koja je dodijelila akademski / stručni stupanj: **Josip Juraj Strossmayer University of Osijek, Department of Physics / Sveučilište Josipa Jurja Strossmayera u Osijeku, Odjel za fiziku**

Permanent link / Trajna poveznica: https://urn.nsk.hr/urn:nbn:hr:160:237200

JOSIP JURAJ STROSSMAYER UNIVERSITY OF OSIJEK

DEPARTMENT OF PHYSICS

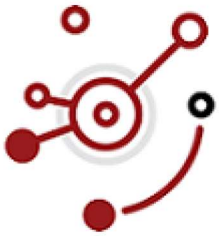

IRENA LUKANOVIĆ

FUSION-EVAPORATION REACTIONS IN THE ^{7}Li + ^{96}Zr SYSTEM

Master's Thesis

Osijek, 2019.

JOSIP JURAJ STROSSMAYER UNIVERSITY OF OSIJEK

DEPARTMENT OF PHYSICS

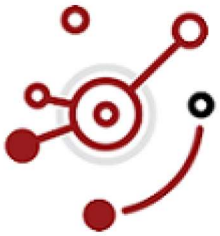

IRENA LUKANOVIĆ

FUSION-EVAPORATION REACTIONS IN THE ^{7}Li + ^{96}Zr SYSTEM

Master's Thesis

submitted to the Department of Physics, Josip Juraj Strossmayer University of Osijek, for the academic degree of Master in Physics and Computer Science Education

Osijek, 2019.

This master's thesis was written in Osijek under the guidance of Maja Varga Pajtler, Ph.D., Assistant Professor, within the Graduate Study in Physics and Computer Science at the Department of Physics, Josip Juraj Strossmayer University of Osijek.

Acknowledgments

Vrata koja vode u život najčešće se otvaraju iza nas, a jedina mudrost za onoga koga progoni miris nevidljivih ruža jest rad.

George MacDonald, *Alec Forbes*, cap. XXXIII

First and formost, I would like to thank my menthor Maja Varga Pajtler, for her patience, support and good guidance, and for always having time for me despite her busy schedule. Special thanks to my sisters, Marina and Ivana, for having ability to make me forget about my problems and always help me with great advices, and my dear Martina, who is always there, despite the distance. You know I always considered you as my sister. Lastly, to my parents, for everything.

To my parents, Ivo and Manda

with love, gratitude and admiration

A. M. D. G.

Contents

Fusion-evaporation reactions in the ^{7}Li + ^{96}Zr system

IRENA LUKANOVIĆ

Abstract

Studying nuclear structure and nuclear reactions and understanding the underlying phenomena causing these processes is essential for gaining knowledge of our Universe. Nuclear reactions and nuclear structure are firmly connected. Through adequate nuclear reaction one can study important properties of nuclei such as binding energies, decay branches, spins and parities. Fusion-evaporation reactions play significant role in studying exotic neutron - rich nuclei. In this experiment the fusion-evaporation reaction $^{7}\mathrm{Li} + {}^{96}\mathrm{Zr}$ at 21 MeV was carried out. More than 90 γ - rays were observed, and 26 of them were associated with four isotopes presented in this work.

The first section of this work deals with a basic understanding of nucleus and nuclear stability with some elementary concepts of radioactive decay, with the emphasis being put on γ - radiation. Interaction mechanisms and basic principles of radiation detectors are discussed in the second section of the thesis. Furthermore, experimental setup, observed γ - ray transitions and analysis of level schemes are presented in the last part of this work.

(42 pages, 26 figures, 1 table, 28 references)

Thesis deposited in Department of Physics library

Keywords: ^{99}Tc, ^{100}Tc, ^{98}Mo, ^{100}Mo, nuclear structure, γ - spectrometry, $\gamma - \gamma$ coincidence, heavy ions, fusion-evaporation reactions

Supervisor: Maja Varga Pajtler, Ph.D., Assistant Professor

Reviewers:

Thesis accepted:

Fuzijsko-evaporacijske reakcije u sustavu ^{7}Li + ^{96}Zr

IRENA LUKANOVIĆ

Sažetak

Proučavanje atomske jezgre i nuklearnih reakcija te razumijevanje osnovnih pojava vezanih uz ove procese važan je način stjecanja znanja o svemiru. Informacije o jezgrama od interesa kao što su energije vezanja, grane raspada (decay branches), spinovi i pariteti mogu se dobiti proučavanjem odgovarajućih nuklearnih reakcija. Reakcije fuzije i evaporacije imaju značajnu ulogu u proučavanju egzotičnih jezgri bogatih neutronima. U ovom je eksperimentu proučavana fuzijsko-evaporacijska reakcija $^{7}\mathrm{Li} + {}^{96}\mathrm{Zr}$ pri energiji od 21 MeV. Od opaženih 90 γ - zraka, njih 26 je pridruženo četirima izotopima prikazanim u ovom radu te su izrađene njihove sheme raspada.

Prvo poglavlje ovog rada bavi se razumijevanjem pojma jezge i njezine stabilnosti, uz elementarne koncepte radioaktivnog raspada s naglaskom na γ - raspad. Središnji dio rada čine mehanizmi interakcija i osnovni princip rada detektora. Eksperimentalni postav i postupak obrade podataka te opažene γ - zrake pridružene pojedinim izotopima objašnjene su u posljednjem dijelu rada.

(42 stranice, 26 slika, 1 tablica, 28 referenci)

Rad je pohranjen u knjižnici Odjela za fiziku

Ključne riječi: ^{99}Tc, ^{100}Tc, ^{98}Mo, ^{100}Mo, atomska jezgra, γ spektrometrija, $\gamma-\gamma$ koincidencija, teški ioni, fuzijsko-evaporacijske reakcije

Mentor: doc. dr. sc. Maja Varga Pajtler

Ocjenjivači:

Rad prihvaćen:

1 General Introduction

One of the main goals of nuclear structure research is to observe and describe the structures and associated symmetries in nuclei in order to understand their properties, which are governed by nucleon - nucleon interactions. Research and development in nuclear physics is significant for our daily lives and has a huge impact on the important advancements in energy, medicine, industry and other sciences. For instance, procedures for testing and treating cancer, localizing tumors, diagnosing Alzheimer's disease and for many other applications are regularly performed in nuclear medicine. Nuclear imaging procedures are noninvasive alternatives to a biopsy and many other surgical procedure and can also give details about the function of almost every major organ system within the body. Although the future direction of nuclear medicine largely relies on advances in nuclear techniques, benefits of nuclear physics go well beyond radiotherapy and diagnostic imaging. Applications of nuclear physics are also used to advance many other scientific fields including climatology, geology and oceanography. The study of nuclear reactions in cosmos is important part of the nuclear astrophysics research. Furthermore, various nuclear techniques are used in industries to polymerize plastics, sterilize food and medical equipment, to embed ions into materials, and to gauge the depth or thickness of materials. Electron beams currently dominate the industrial uses which leads to many possibilities for development of the nuclear physics in the near future, especially with the emergence of new generations of exotic beam facilities.

In order to accelerate scientific progress, it is important to advance our understanding of the nuclear structure. The main goal is to explain the organization and properties of nuclear matter and how they interact. Modern research is developing through two approaches: a microscopic perspective focusing on the motion of individual nucleons and their interactions, and a macroscopic one that focuses on a collective behavior of nucleons.

1.1 Nuclear structure

The question that has been primal to nuclear physics since the beginning was: How does subatomic substance organize itself and what phenomena appear? Understanding nuclear

physics and what goes on within the nuclei includes understanding the structure of nuclei and their components, as well as understanding the phenomena that occur when many of them get together.

In the late 19th century the structure of an atom was still unknown and during this time the first models of an atom began to emerge. The existence of the positive charge densely concentrated at the center of the atom in the form of a nucleus was first proposed by Ernest Rutherford in 1911 [1]. His model is based on the gold foil experiment with a beam of α particles, through which he came to the conclusion that most of the mass of an atom is concentrated in its nucleus, which is extremely small compared to the size of the atom. In the 20th century all subatomic particles were already experimentally discovered and better models of an atom were developed, among which the most famous models were Bohr's and the quantum mechanical model.

Nucleus is usually considered simply as a system of positively charged protons and uncharged neutrons, which are both called nucleons. The size of the nucleus is namely about 10^{-12} to 10^{-13} cm in diameter and can include several hundreds individual protons and neutrons that interact mainly through the nuclear and Coulomb forces[1]. The number of neutrons with a given number of protons in a nucleus can differ significantly. Although there are 118 different elements in the periodic table so far - there are far more isotopes than elements.

It is impossible to see subatomic particles directly, yet, it is possible to obtain knowledge of their structures by observing the results of nuclear reactions. They are dictated by the atomic nuclei, since it is their charge that determines the electronic structure. There are two main kinds of nuclear reactions - radioactive decay and nuclear transmutation reactions. Radioactive decay is a spontaneous transformation of an unstable nucleus which results in the emission of particles or electromagnetic radiation. The vast majority of nuclei are unstable and they display a spontaneous disintegration of the nucleus. The stability of the nucleus is based on the number of protons and neutrons in the nucleus, therefore, nuclei are usually represented on the Z, N chart of the nuclides which shows the relative stability of different isotopes (Figure 1.1.1). The dark marks represent the most stable isotopes of any given element, also known as the valley of stability. The coloured marks are associated with less stable or unstable isotopes of given element.

[1]The attractive nuclear force is stronger than the repulsive Coulomb force which is of the same order as the size of light nuclei i.e. approximately 2 to 4 fm and binds nucleons together. In addition, electromagnetic and weak interactions are responsible for the dominant decay processes while gravitational forces can be ignored in the nuclei.

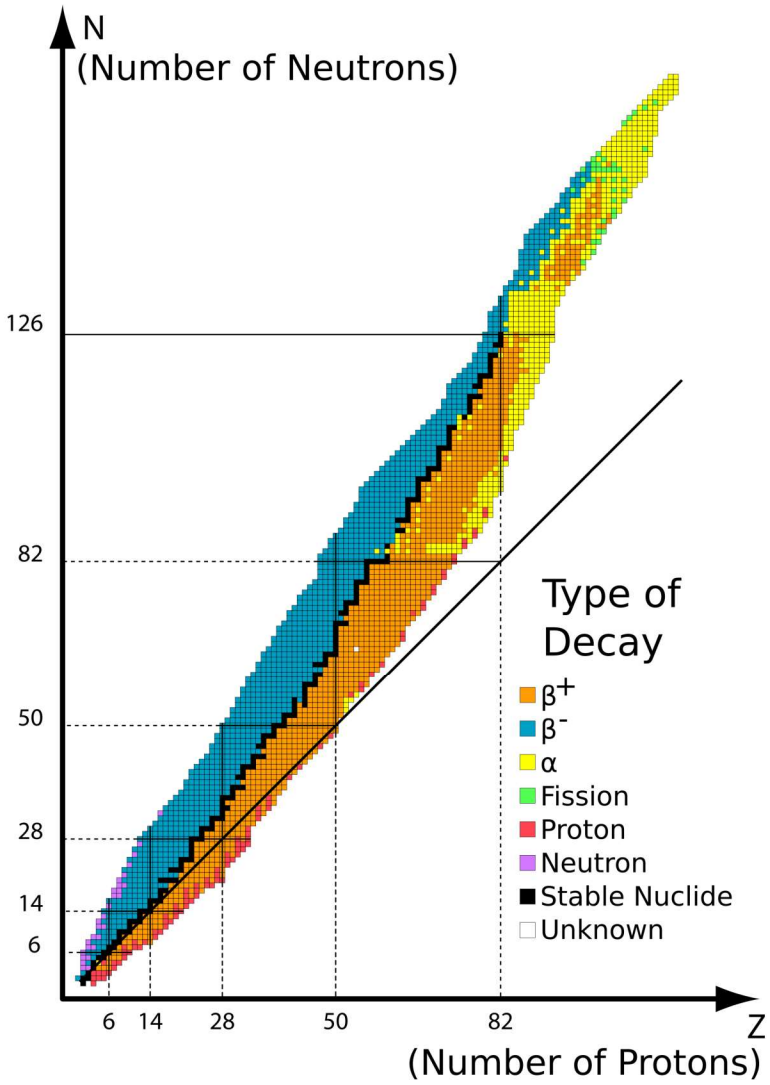

Figure 1.1.1: Chart of nuclides by type of decay [2]. The diagonal line corresponds to balanced numbers of protons and neutrons. Nuclides with excessive number of neutrons or protons are unstable and undergo β decay (orange and blue region). At high atomic number, alpha emission (yellow region) becomes a common decay mode. Another reaction mode for the nuclei at the top of the chart is the fission, which is associated with green region. Red and violet region represent proton and neutron decay, respectively.

The valley of stability represents the location of stable nuclei in the Z, N chart, therefore, it is energetically favorable for nuclei far from the valley to move towards it through nuclear decay, in the ways described in the subsection 1.3. Radioactive decay is determined by mass change - daughter nuclei always have a smaller mass (i.e. lower energy) than the parent nucleus. There are some important points of nuclear stability that need to be addressed:

1. It has been observed that elements with an even number of protons (Z) generally have more

stable nuclides than elements with an odd Z.

2. Heavy stable nuclides have more neutrons per proton compared to the light nuclides.

3. More than half of the stable nuclides have even values of both N and Z. Only four nuclides with odd number of protons and neutrons are stable: ${}^{2}_{1}\mathrm{H}$, ${}^{6}_{3}\mathrm{Li}$, ${}^{10}_{5}\mathrm{B}$, ${}^{14}_{7}\mathrm{N}$.

Any combination of protons and neutrons will belong to one of the three main types of nuclei: stable, radioactive (unstable but bound nuclei) and unbound nuclei. By adding protons or neutrons to a stable nucleus, one enters the region of radioactive nuclei, after which one attains the nuclear drip line [3]. Drip line defines the limit between bound and unbound nuclei. This means that nuclei are no longer bound by the strong force i.e. binding force is not enough to prevent nucleons from dripping off the nuclei. Boundary between bound and unbound nuclei is determined by the separation energy of isotopes where separation energy represents minimum energy required to remove nucleon from the nucleus. Neutron drip line is the boundary for the neutron - rich nuclei at which any more neutron added to the nucleus will not be bound i.e. neutron separation energy becomes negative. Stability of superhaeavy nuclei, their lifetimes and their precise location in the Z,N chart is important area of study and is yet to be investigated. One way to produce and observe heavy elements is by using neutron - rich radioactive nuclei and beams that would decay through the evaporation of the extra neutrons into the superheavy ground state [3].

1.2 Nuclear shell model

Nuclear shell model is one of the models of nuclear structure which predicts the existence of stable nuclei. It was developed by Wigner, Goeppert - Mayer and Jensen during the 20th century and it is based on the idea that some nuclei are bound more tightly together compared to the other ones, which results from filling the nucleon energy levels [4]. Numbers 2, 8, 20, 28, 50, 82, 126 are called magic numbers and nuclei with any of these numbers of neutrons or protons are very stable. In addition, numbers 40 and 64 are weakly magic over restricted ranges of N and Z [5]. The magic numbers manifest themselves in many nuclear properties, such as masses, particle separation energies, electric quadrupole moments, etc. Although nuclear shell model differs from atomic model [2], nuclear energy levels are similar to electron energy levels in a way that a filled shell results in better stability. The concept of magic numbers and nuclear shells is illustrated in

[2] In atomic model electrons are arranged in shells around the atomic nucleus.

Figure 1.2.1.

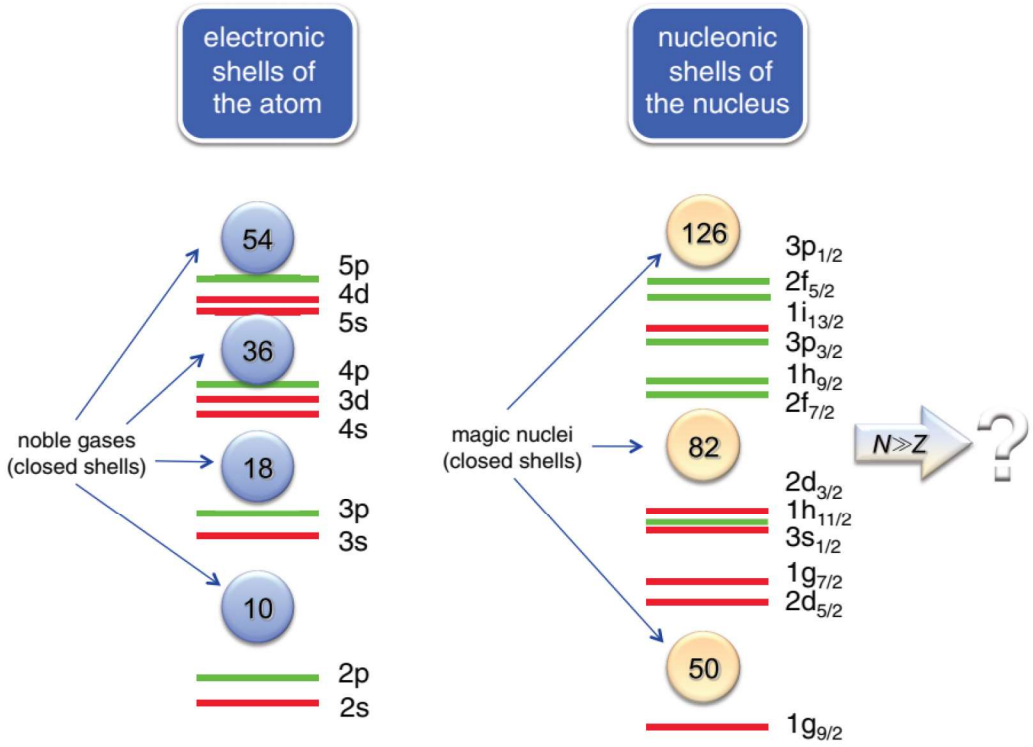

Figure 1.2.1: Shell structure in atoms (left) and nuclei (right) [6]. Atomic shell structure is formed of energy levels where each electron shell has a different energy level. Nuclear shell structure of stable nuclei is shown on the right. It is noted that shells of nuclei with proton or neutron numbers 2, 8, 20, 28, 50, 82 and 126 are entirely filled. On the other hand, shell structure of very neutron rich nuclei is unknown [7].

It is well known that the interaction of each nucleon with its neighbors within the nucleus can be described by some average potential $V(r)$. A single nucleon moves independently in this potential and can be portrated by a single - particle state of discrete energy and constant angular momentum. In the simplest case, it consists of a central potential and a strong spin – orbit coupling term. The solutions of the Schrödinger equation for such a potential are bound single - particle states that are characterized by the values of the radial quantum number n, orbital angular momentum quantum number l, and total angular momentum quantum number j [3]. Therefore, the single - particle states are determined with the values of n, l and j. Shell structure is consisted of single - particle states energetically gathered in groups. Each state of given j can be occupied

[3]Total angular momentum quantum number j (also known as the first total angular momentum quantum number) is given by $\vec{j} = \vec{l} + \vec{s}$, where s is the intrinsic spin equal to $\frac{1}{2}$ for protons or neutrons.

by a maximum number of $(2j+1)$ identical nucleons where secondary total angular momentum quantum number is $m_j = -j, -j+1, ..., j-1, j$, which constitute a subshell [4]. The shells are filled in a way that nucleons obey the Pauli exclusion principle [5].

Nuclear shell model has been used as a template to view nuclear structure since the middle of the 20th century. However, ground states or low-energy excitations in many nuclei involve a coordinated motion of many nucleons and shell model description is not adequate for nuclei in which the valence nucleons occupy more than one j shell. Therefore, other theoretical models have been developed. One of the models used to explain and describe the nuclei with many valence nucleons is collective model which assumes that nucleons inside the nucleus are acting together and collide regularly with each other. Different collective motions such as rotations and vibrations can occur in nuclei, and collective model emphasizes coherent behaviour of all of the nucleons. This model has been successful in predicting nuclear properties in deformed regions i.e. for nuclei far from the doubly magic regions.

1.3 Types of decay

Nuclides can decay in several ways. There are three natural types of radioactive decay that are introduced in the table 1.3.1.

Table 1.3.1: Types of radioactive decay

Decay	**Parent nucleus**	**Daughter nucleus**	**Radiation**
α	Z/N	$Z-2/N-2$	^{4}He nucleus
β^-	Z/N	$Z+1/N-1$	electron
β^+	Z/N	$Z-1/N+1$	positron
γ	Z/N	Z/N	γ - photon

The modes of radioactive decay are primarily α and β decay, and rarely spontaneous fission. α decay includes a heavy unstable nucleus that rejects the α particle which is identical to the ^{4}He nucleus. With this in mind, α emission is the most common way for a heavy nucleus ($Z > 83$) to

[4] Secondary total angular momentum quantum number m_j (also known as projection of total angular momentum) m_j ranges from $-j$ to j in steps of one.

become more stable [6]. An example of a α decay is the decay of radium ^{88}Ra which yields radon.

$$^{226}_{88}\mathrm{Ra} \longrightarrow ^{222}_{86}\mathrm{Rn} + ^{4}_{2}\alpha$$

β decay includes three modes: β^- decay, β^+ decay and electron capture. Conversion of neutron into proton which generates fast electron and neutrino is called β^- decay. Therefore, it results in a daughter nuclide with the next higher atomic number. Example of β^- decay is decay of ^{14}C that is used in radiocarbon dating.

$$^{14}_{6}\mathrm{C} \longrightarrow ^{14}_{7}\mathrm{N} + ^{0}_{-1}\beta$$

$$n \longrightarrow p + e^- + \bar{\nu}$$

On the other hand, β^+ decay includes conversion of proton into neutron along producing fast positron and antineutrino. It has the opposite effect of β^- decay, i.e. daughter with the next lower atomic number is formed. Radioactive ^{11}C becomes stable ^{11}B through β^+ emission.

$$^{11}_{6}\mathrm{C} \longrightarrow ^{11}_{5}\mathrm{B} + ^{0}_{1}\beta$$

$$p \longrightarrow n + e^+ + \nu$$

During electron capture (EC), the nucleus interacts with an electron in a low energy state. Combining proton with electron results in forming a neutron which is accompanied by the emission of a neutrino. The orbital vacancy is either filled by an electron from a higher energy state with the emission of Roentgen rays - or by the ejection of an outer electron (the so - called Auger effect). After the α or β decay the daughter nucleus is usually in one of the excited states and it can discard excess energy by γ decay. Therefore, γ emission is a result of the transitions between the excited states of nuclei. Since γ decay does not produce a new element, it is not a decay process per se, yet it is the de-excitation of nucleus. Atomic nuclei occur in a particularly wide range of masses and electric charges and it is important to emphasize that a particular nucleus may decay by more than one mode.

Nuclear decay occurs naturally under all circumstances, while transmutation of nucleus requires special environment and conditions to happen. For example it happens in the interior of

stars or during collision of a beam of highly energetic particles with a target nucleus. Transmutation includes nucleus that react with a subatomic particle or another nucleus to form a product that is more massive than the starting material.

1.4 Types of direct reactions

Nuclear reaction includes a conversion of at least one nuclide to another. In contrarily, if there is no transformation after the interaction, the process is known as nuclear scattering, rather than a nuclear reaction. Well - known examples of nuclear reactions are fusion and fission. While fusion reactions occur in stars, most famous type of reactions that is man - controlled is fission, which occurs in nuclear reactors.

Basic classification of nuclear reactions in terms of the interaction time is direct and compound nucleus reactions. If the reaction takes place within the time scale of 10^{-22} s or less, it is called direct nuclear reaction. In direct reactions only few degrees of freedom are excited while other degrees of freedom stay effectively passive [8]. On the other hand, non direct compound reactions are slower because intermediate compound nucleus requires longer interaction time, i.e. $\gg 10^{-22}$ s and they involve large number of interactions between nucleons. Thus the compound nucleus reactions include excitations of many degrees of freedom and these reactions usually occur if the projectile has low energy.

Classes of direct reactions are elastic and inelastic scattering, capture reactions, transfer reactions, breakup reactions and knock - out reactions.

Elastic scattering is "the simplest reaction" in which a projectile and a target stay in their ground states and there is no energy released during the reaction. Particles in the collision only change their direction of motion and maybe spin orientation [8]. On the other hand, if projectile and target nucleus are complex, they can be left in excited states, which is know as mutual excitation. We can learn about the size and structure of nuclei by observing how the nuclei deflect the incident particles. A reaction where a projectile or a target is left in excited state is known as inelastic scattering. Unlike elastic scattering, energy in this type of reaction is transferred between the target nucleus and the incident particle.

Reactions where charged or neutral particle is captured by nucleus are known as capture reactions and they are accompanied by the emission of γ - rays.

Another class of reactions that lead to transmutations are transfer reactions. Type of reaction where one or more nucleons are transferred between target and passing particle are called particle transfer reactions. They are further arranged as:

1. Stripping reaction (d,p) – one or more nucleons are transferred from the projectile to the target, for example:

$$^{90}_{40}\mathrm{Zr} + d \longrightarrow ^{91}_{40}\mathrm{Zr} + p$$

2. Pickup reaction (p,d) - one or more nucleons are transferred from the target to the projectile, for example:

$$^{16}_{8}\mathrm{O} + d \longrightarrow ^{15}_{8}\mathrm{O} + ^{3}_{1}\mathrm{H}$$

Breakup reaction is type of reaction in which projectile breaks into two or more fragments, which is no longer a simple two - body process.

A reaction were projectile collides with the target and a single nucleon or a light cluster is removed from the projectile is known as knock - out reaction.

1.5 Fusion-evaporation reactions

Fusion-evaporation reactions are usually used to produce heavy elements. In these types of reactions heavy-ion projectile a collides with heavy target nucleus A to form a compound nucleus C^*. Compound nucleus C^* is in excited state and it loses energy through evaporation process, which leaves the nucleus in the excited state and it de-excites by γ - radiation. Light particles b, such as neutrons, evaporate and this way produce the nucleus of interest B, as shown in the following equation:

$$a + A \longrightarrow C^* \longrightarrow b + B^* \longrightarrow b + B + \gamma$$

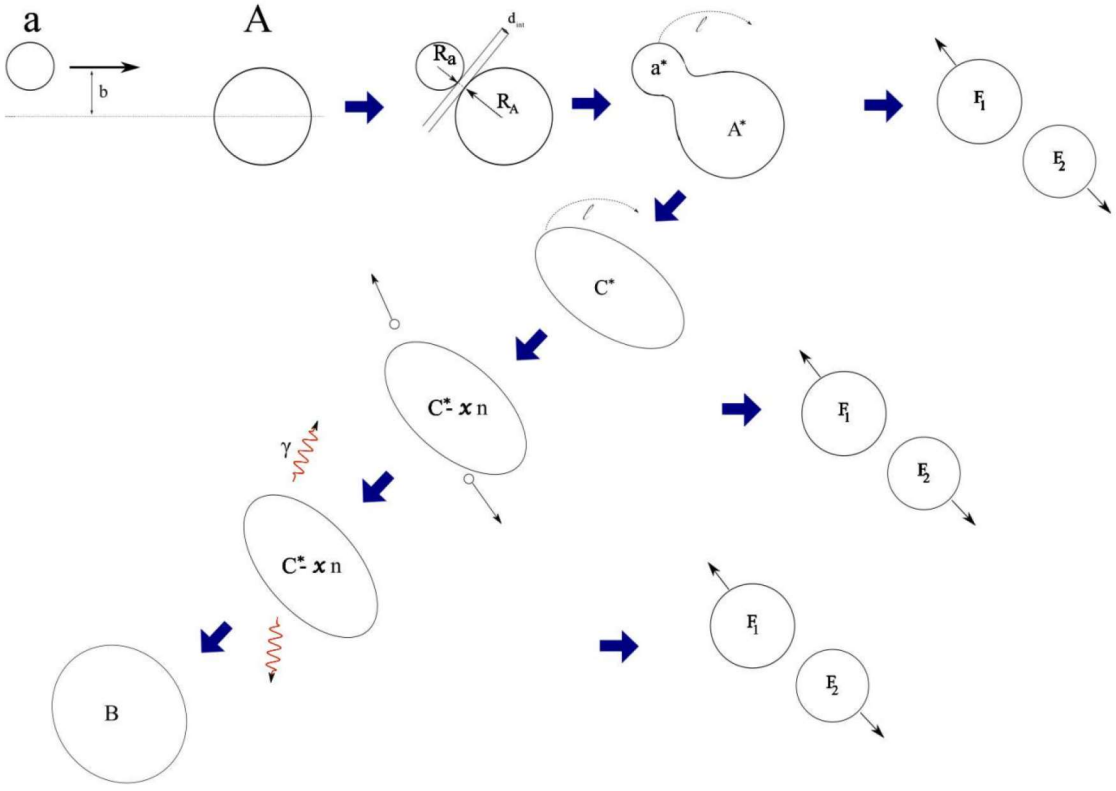

Figure 1.5.1: Schematic representation of fusion-evaporation process. The projectile a and the target A collide with the impact parameter b. The compound nucleus C^* is formed through fusion. It is also possible for the system to go through fission, i.e. decompose in two fragments F_1 and F_2. Compound nucleus can lose energy through evaporation of neutrons and γ - rays and this way forms the evaporation residue B [9].

This reaction is a multi-step process (Figure 1.5.1) which can be divided in the following steps:

1. Contact and capture between projectile and target;

2. Fusion - formation of the compound nucleus;

3. Evaporation of particles to form the nucleus of interest;

4. Emission of γ - rays in the decay to the ground state;

Coulomb repulsion is proportional to:

$$\frac{Z_a Z_A}{\mathrm{A}_a^{1/3} + \mathrm{A}_A^{1/3}}$$

where Z_a, A_a, Z_A and A_A are the charge and mass number of nuclei a and A [9]. Projectile and target need to overcome Coulomb barrier in order for capture to happen, i.e. the energy in the center of mass must be above this value. On top of that, following conditions in terms of the size of nuclei and angular momentum need to be met:

1. The distance between the two centers at contact is $b_{contact} = R_a + R_A + d_{interaction}$, where R_a and R_A are the radius of the nucleus a and A, respectively, and $d_{interaction}$ the distance of interaction of these nuclei [5]. The impact parameter must be smaller than the value $d_{interaction} \approx$ 2 - 3 fm in order for nuclei to touch.

2. The transferred angular momentum in the reaction is given by $\sqrt{l(l+1)} = \frac{\mu v b}{\hbar}$, where l is the angular momentum, μ is the reduced mass of the system [6], v is the speed of the projectile and b is the impact parameter. For very large angular momentum l corresponding impact parameter is large, and disfavours the contact.

The formation of the compound nucleus C^* will depend on the beam energy E, the angular momentum l and the entrance channel. If the formation doesn't succeed, pre-compound system $a + A$ will split into target-like and projectile-like fragments, which is known as quasi-

[5] The radius of a nucleus is given by $R = R_0 A^{1/3}$, where $r_0 = 1.2$ fm.

[6] Reduced mass of the system is given by $\mu = \frac{m_a m_A}{m_a + m_A}$, where m_a and m_A are the masses of the nuclei a and A.

fission (Figure 1.5.1) [9].

After compound nucleus C^* is formed, it is in excited state, where excitation energy of nucleus is:

$$E^* = E_{cm} + Q.$$

Q is the Q-value of this reaction and it is determined with:

$$Q = BE_{CN} - (BE_a + BE_A).$$

E_{cm} represents the total energy available in the center-of-mass frame, E_{CN} is the excitation energy of compound nucleus and B is the fusion barrier height [9]. Compound nucleus can lose energy through evaporation of particles such as neutrons and γ - rays. Evaporation of neutrons is preferred to protons and α particles since it is not influenced by the Coulomb barrier. Consequently, mainly neutron-deficient isotopes are produced. This way excitation energy is reduced by the separation energy and the kinetic energy of the evaporated particle. Emission of γ - rays brings nucleus closer to the yrast line (state with minimum energy) until the yrast line is reached and after that, nucleus decays along the yrast line towards the ground state [10].

2 Radiation interaction with matter

2.1 Radiation interaction with matter

There are several fundamental mechanisms by which radiations can interact with matter and lose energy. In general, result of the radiation interaction with matter is partial or full energy transfer from the incident particles to the particles of the absorber material (electrons or nuclei). Two categories of radiation, heavy charged particles and fast electrons, continuously interact through the Coulomb force with electrons present in any medium they go through. On the other hand, uncharged radiations such as neutrons, X - rays and γ - rays, are not subject to the Coulomb force. These uncharged particles can pass completely through the detector without any evidence of their existence except in the case where radiation includes radical change of the properties of the incident radiation, so called catastrophic interaction. Through several processes such as photoelectric effect, Compton scattering and pair production, γ - rays can transfer their energy to medium particles.

Interaction of heavy charged particles with matter is based on the Coulomb forces between positive and negative charges of the incident and absorber atoms. When charged particle enters absorbing material, it interacts with many electrons in material at once. Due to attractive Coulomb force in all these encounters, atom may be excited to a higher energy level or be ionized[7] (Figure 2.1.1.). Results of these interactions are either excited atoms or ion pairs which includes free electrons and the positive ions of absorber atoms. Electrons in outer shells are mainly ionized and ionization of inner-shell electrons is generaly very small. In comparison with heavy charged particles, fast electrons lose their energy at lower rate. Another difference is that energy loss may take the form of not only Coulomb interactions but also radiative losses such as bremsstrahlung[8] or electromagnetic radiation (Figure 2.1.1.). This happens when charged particle penetrates the atom and interacts with its nucleus. However, it is important to emphasize that radiative losses represent only small part of the energy losses and are important only in materials of high atomic number [11].

Interactions of γ - photons with mater don't include direct ionization of atoms as heavy-

[7] Ionization means to completely remove electron from the atom.

[8] Bremsstrahlung is the radiation given off by a charged particle due to its acceleration as a result of an electric field of another charged particle (most often an atomic nucleus).

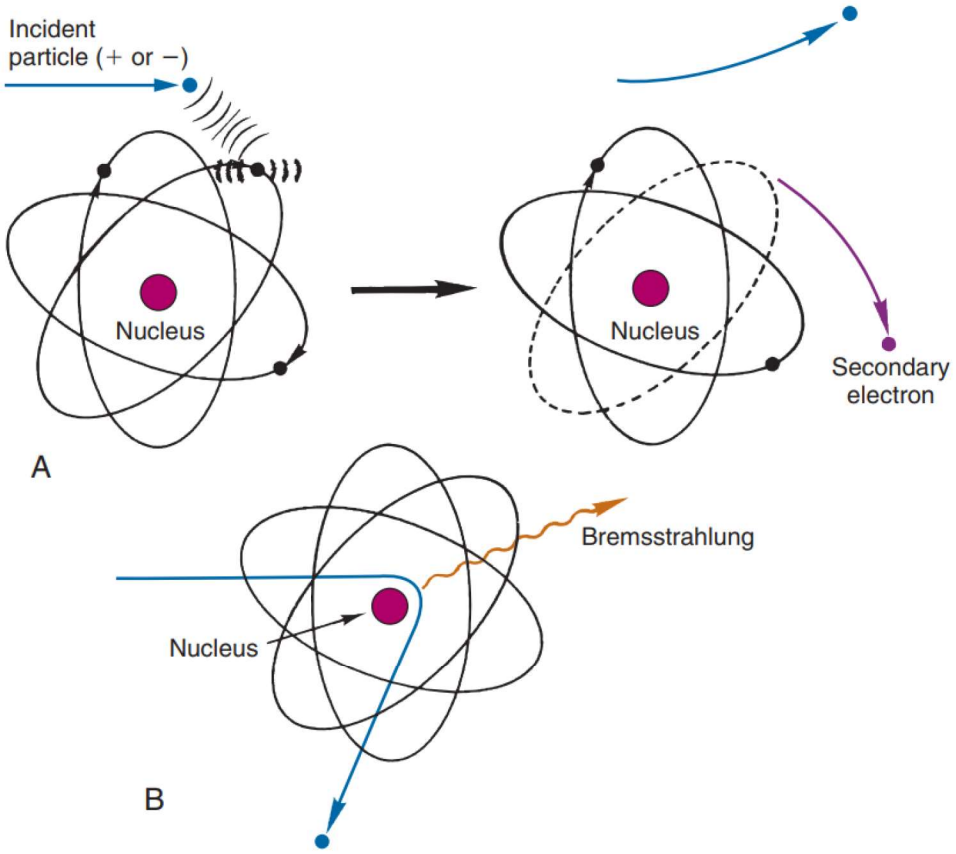

Figure 2.1.1: Interactions of charged particles with matter. A) Ionization is associated with a collision between the charged particle and an orbital electron. Part of the energy of charged particle is used to overcome the binding energy of the electron to the atom, and the rest represents kinetic energy of the ejected secondary electron. B) Interaction with a nucleus, resulting in bremsstrahlung production. Incident particles are negative in case A) and positive in case B) [12].

charged particles mechanisms do. In radiation measurements of γ - rays three interaction mechanisms are most important: photoelectric effect, Compton scattering and pair production. Result for all these processes is energy transfer from γ - ray photon to electron by which photon either disappears completely or is scattered.

2.2 Interaction mechanisms for γ - rays

Photoelectric effect is predominant way of energy transfer for γ - photons with relatively low energy. It is the process in which photon interacts with absorber atom and it completely disappears. Absorption leads to ejection of photoelectron from one of atoms shells, most often K shell of the atom, which is most tightly bound. In order photoelectric effect to

happen, incident photon needs to have higher energy than the biding energy of the shell. Energy of photoelectron E_e is determined by the equation:

$$E_e = h \cdot f - E_b$$

where $h \cdot f$ represents original photon energy and f stands for frequency of incident photon. E_b is the binding energy of photoelectron in its original energy level [11]. Ejection of photoelectron creates a hole in electron shell which can be filled with emitted electron from other shell. Therefore, one or more X - ray photons may be produced beside photoelectron through rearrangement of electrons from other energy levels or capture of a free electron (Figure 2.2.1. a)).

Compton scattering is the process where incident γ - ray photon is deflected through an angle θ compared to its original direction due to the collision with the electron that is initially at rest (Figure 2.2.1. b)). This electron belongs to outer shell of an atom. Energy of photon is transferred only partially to the stationary electron and it can vary from zero to a large fraction of the γ - ray energy [11].

$$h \cdot f^{'} = \frac{h \cdot f}{1 + \frac{h \cdot f}{m_0 c^2} \cdot (1 - \cos\theta)}$$

where $m_0 c^2$ represents the rest - mass energy of the electron and is 0,511 MeV. Frequency of the photon after scattering is labeled as $f^{'}$ [12].

If γ - ray photon has energy twice the rest - mass energy of an electron, third type of interaction mechanism is possible. Pair production occurs when photon enters electric field of charged particle, it disappears and pair electron - positron is created. Positron loses all of its kinetic energy and is stopped. Secondary products of pair production are two annihilation photons that usually travel some distance before another interaction. This process becomes more important with higher photon energies (Figure 2.2.1. c)).

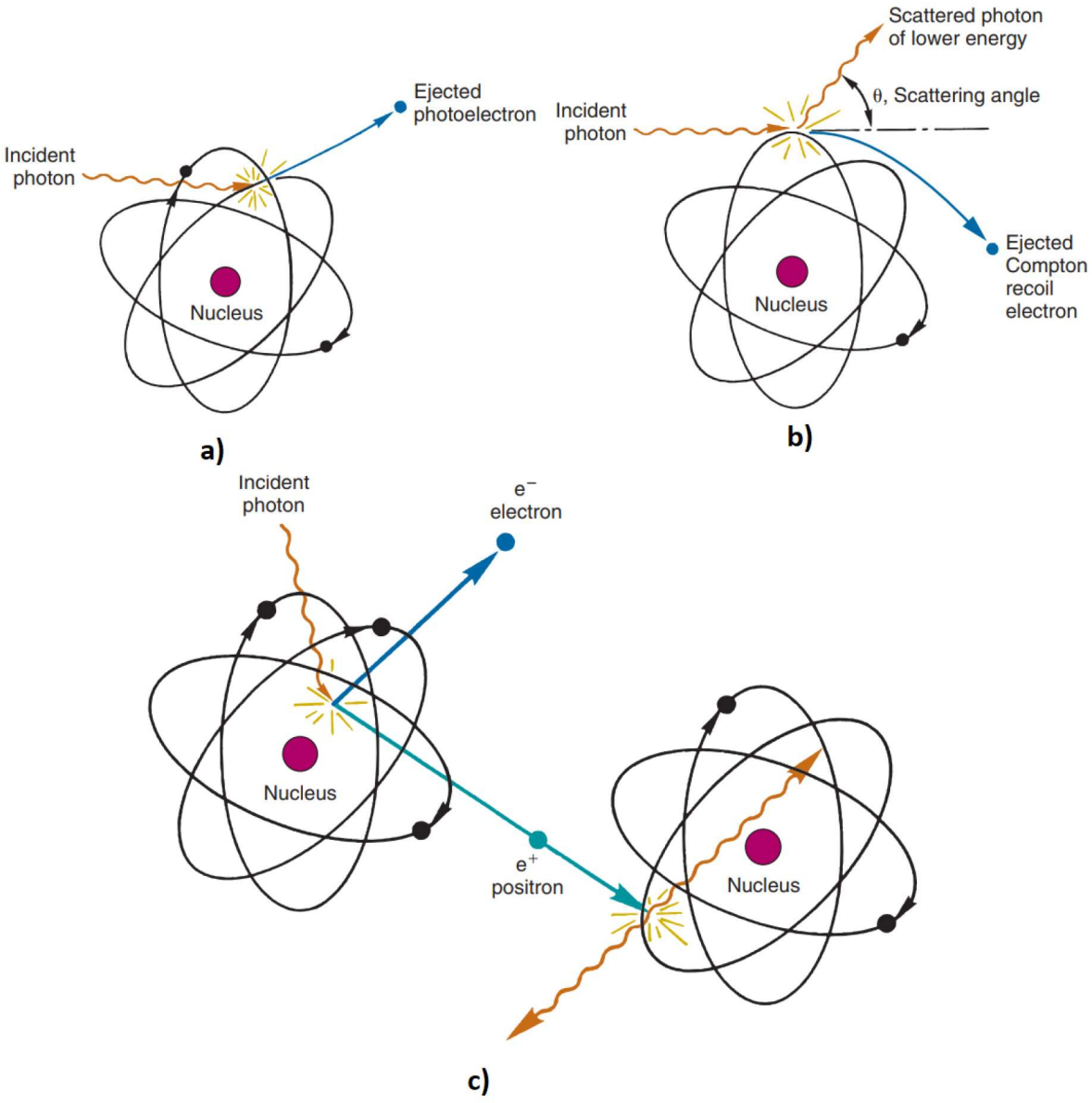

Figure 2.2.1: Schematic representation of a) photoelectric effect, b) Compton scattering and c) pair production. In the photoelectric effect the incident photon transfers its energy to a photoelectron and disappears. In Compton scattering the incident photon transfers part of its energy to an electron and is scattered in another direction of travel. In pair production energy of incident photon is converted into an electron and a positron (equivalent to energy of 1.022 MeV) and their kinetic energy [12].

3 Detectors in experimental nuclear physics

There are various types of detectors which differ in their application and way of working. They are usually categorized by either the type of detector element that is used or by their function involved. Essentially, it is possible to directly detect only the electric impulse of a detector which may contain informations about the existence of radiation (for example the Geiger - Muller tube), the energy of the detected particle, the time of detection, the position of detected particle and the type of radiation. All other information is obtained from these detected units. One of the common ways of capturing some sort of data from radioactivity in the early years was the photographic plate and later the electroscope. The electroscope had a better level of sensitivity than photographic plates. It could be set up to measure alpha or β particles and it was important for the early experiments involving radioactivity. The spinthariscope, cloud chambers, and many other early devices were significant in learning the basics of radiation and carrying out important experiments that set the stage for later developments. This led to new types of detectors such as the Geiger - Muller tubes, the ion chamber and scintillators, which are nowadays still in use.

Today there are three types of radiation instruments with their specific strengths and weaknesses: gas - filled detectors, scintillators, and solid state detectors. Gas - filled detectors are used most often. Most common gas - filled detectors include ionization chambers, proportional counters, and Geiger - Mueller tubes, which function in a similar way. They consist of a gas chamber between two electrodes which give voltage i.e. a difference in electrical potential. The gas becomes ionized when it interacts with incident radiation i.e. ion pairs are created within the gas. The ion pairs move towards the opposite electrodes and the electrometer measures the ionization current. One of the main disadvantages of the ionization - chambers is that it cannot distinguish the types of radiation and it cannot enable an energy spectrum. These three types have a different applied voltage across the detector which specifies the type of response that detector will register. The Geiger - Muller tube operates at much higher voltage than the other two and is used as a simple counting device to measure count or dose rates.

Most of the penetrative γ - rays would pass through gas - filled detectors without any interaction and be, therefore, unregistered. One of the essential properties for gamma detection is to have a detector made of dense material. Nowadays, semiconductor detectors and scintillation detectors are standard detectors for detecting γ - rays.

3.1 Scintillation detectors

Scintillation detectors consist of scintillators - transparent materials that can be solids, liquids or gases - and light sensors - photomultiplier tubes and photodiodes which are used to convert the light into a voltage pulse. Scintillators are based on scintillation which occurs when ionizing radiation passes through these materials so they may be used as detectors when they are exposed to radiation. The aim is to produce a large light output in a visible range. In order to gain a better voltage pulse, scintillation materials should be transparent to the wavelength of their own emitted light so light can be propagated. Other preferable properties of scintillation materials are as follows:

- the kinetic energy of charged particles should be converted into observable light with a high scintillation efficiency.
- the light conversion should be linear.
- the time of de-excitation and photon emission should be short in order to generate fast signal pulses.
- the material should be of good optical quality and its index of refraction should be near 1.5 to enable an efficient photon interaction with light sensors [12].

All these properties cannot be found in one material only. Instead, there are organic and inorganic scintillation materials used for detection that meet different criteria. Some of the inorganic crystals are NaI(Tl), CsI(Tl), CaI(Na), LiI(Eu) and CaF_2(Eu). Generally speaking, inorganic crystals have a better light output and linearity, but a bigger response time compared to organic ones. In addition, the type of material plays a significant role in detecting the emitted light. The high atomic number and the high density of inorganics make them a better choice for γ - ray spectroscopy, whilst organics are used for β spectroscopy and the detection of neutrons. Some organic materials with the high concentration of hydrogen atoms that are used for detection of fast neutrons are antracene, stilbene and doped p-terphenyl.

The scintillation in inorganic crystals occurs due to the structure of the crystal lattice and is different from the one in organic crystals. In organic crystals the process of fluorescence, in which visible light is emitted from the material after its excitation, is independent of its physical

state because it arises from the transitions of the energy level structure of a single molecule. An example of an organic scintillators with π-electronic structure [9] is shown in Figure 3.1.1. The upward arrows represent the absorption of kinetic energy of charged particles i.e. the excitation process, and the downward arrows indicate the emission of radiation i.e. the de-excitation process.

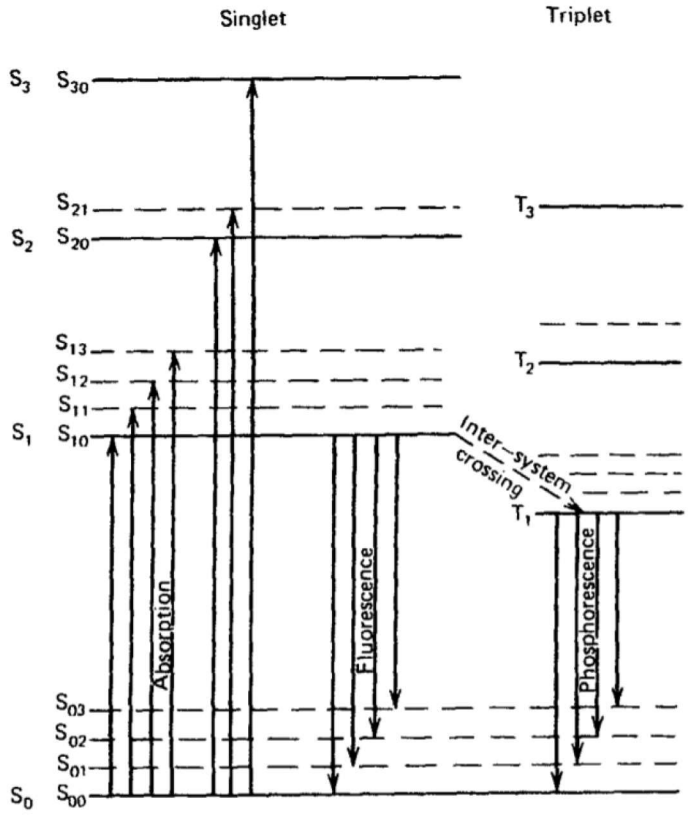

Figure 3.1.1: π-electronic configuration of an organic molecule [13]. Set of singlet ($S = 0$) and triplet ($S = 1$) states are labeled as S_0, S_1, S_2... and T_0, T_1, T_2 respectively.

The scintillation mechanism occurs as follows: at room temperature all molecules are in the S_{00} state. When a charged particle passes through, its energy is absorbed by the molecules, which leads to the excitation of electrons. Electrons in the higher states S_2 and S_3 lose energy through internal conversion to the S_1 state (in picoseconds). Also, states that are not in thermal equilibrium with their neighbours such as S_{11} and S_{12} quickly lose extra energy. $T_1 \rightarrow S_0$ transitions represent delayed light emission (phosphorescence). In addition, the T_1 state lies below the

[9] π-structure is determined by π bond which is formed by the overlap of orbitals in a lateral fashion with the electron density concentrated above and below the plane of the nuclei of the bonding atoms [14].

S_0 state. Therefore, the phosphorescent and the scintillation light are different, based also on their wavelength.

In inorganic scintillators the energy levels are determined by the structure of the crystal lattice. As shown in Figure 3.1.2., the energy band structure consists of a valence band (electrons are bound to lattice atoms and can't move), a conduction band (some electrons have enough energy to be free from parent atoms and to move through crystal) and a forbidden area between them, in which electrons can never be found in pure crystal. When an electron in the valence band absorbs energy, it can move to the conduction band leaving a void behind it, also known as a hole [10]. The excitation process is followed by an emission of a photon, although the width of the band gap in a pure crystal is usually such that the emitted photon isn't in the visible range of the spectrum. Therefore, a small amount of impurities (also known as activators) is added to the inorganic scintillators in order to modify the energy structure at the activator location (although the crystal in general is not modified). Consequently, energy states also known as recombination centres will be created in the forbidden area, which generates visible photons during the de-excitation process. For this reason activators such as Tl, Na and Eu are usually added to the alkali halides such as NaI, CsI, CaI, LiI and CaF. The excited energy states in forbidden area are shown in Figure 3.1.2.

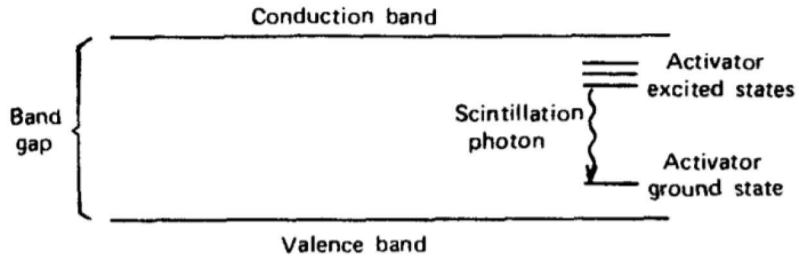

Figure 3.1.2: The energy band structure of an activated inorganic scintillator [13]. De-excitation of electrons occurs through activation states within forbidden band.

The scintillation light is converted to the electronic signal with the photomultiplier tube and the photodiode. This process is illustrated in Figure 3.1.3.

1. When a charged particle migrates through the crystal, it creates a large number of electron-hole pairs. Holes will drift to the activator location and activator sites will become ionized. After the absorption of incident energy and the excitation, de-excitation will occur so that the emitted photon

[10]Holes represent the absence of electrons. They contribute to the conduction the same way electrons do.

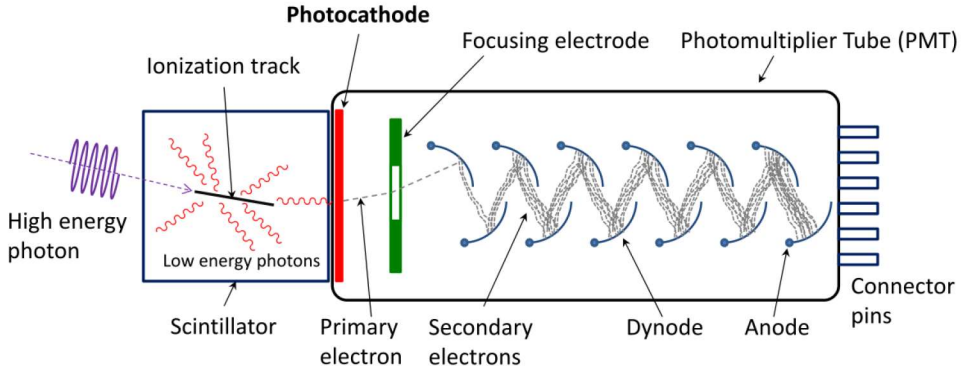

Figure 3.1.3: Main elements of scintillator detector [15].

is visible.

2. The emitted photon is guided to a photomultiplier tube (PMT) where it interacts with the photocathode of PMT which results in releasing electrons (Figure 3.1.3). These electrons from the photocathode are guided with the help of an electric field. They move towards the first dynode where the secondary electrons are emitted [11]. The secondary electrons are guided towards the second dynode and the successive process repeats until the last dynode i.e. anode. The final amplification is about 10^6 or higher. The main reason PMT is necessary is because the primary signal out of the scintillation material is low. On the other hand, a large amplification leads to a poor energy resolution.

Lanthanum Bromide ($LaBr_3(Ce)$) scintillation detectors are one of the newer inorganic scintillation detectors for γ - ray detection. LaBr detectors provide a better energy resolution, pulse shape and temperature stability compared to NaI(Tl) detectors [16].

Figure 3.1.4: LaBr detector [16].

[11] Dynodes are coated with a substance that emits secondary electrons.

Also, the size of the scintillator is important, just as the thickness of the scintillation material, it defines its ability to absorb and detect certain emission rays. A thin scintillator is good for detecting low-energy γ - photons and high - energy β particles, while high-energy γ - photons would pass through the thin scintillator without interacting. If the material is thick enough, it could detect high-energy γ - rays, but it is not very good for low-energy γ - rays since it will absorb the produced light before it can be detected.

3.2 Semiconductor detectors

Metals, insulators and semiconductors differ in electrical conductivity behaviour which depends on the energy gap between valence and conduction bands in the material. Semiconductor detectors, also known as solid - state detectors, are based on semiconductor material such as silicon and germanium which are used as detecting medium. Main information carriers in semiconductor materials are electron - hole pairs. Sufficient energy needed to create electron - hole pair depends on the energy gap between valence and conduction bands in the material which is different for different type of semiconductor material. Energy band gap for predominant cases, silicon and germanium, is about 1.1 eV and 0.7 eV, respectively [17]. However, semiconductors with added impurities (extrinsic or doped semiconductors) have few advantages. In pure crystals there are no available energy levels between conduction and valence bands. Therefore, intrinsic semiconductors have extremely low concentrations of charge carriers. However, by doping the material i.e. adding impurities to semiconductor, conductivity can be increased significantly. It is altered because additional levels in forbidden band are created [12] which might capture electrons from the conduction band or holes from the valence band. By adding electron donor sites to intrinsic semiconductor, it becomes a doped n - type semiconductor (n^+ semiconductor). On the other hand, doping intrinsic sample with acceptor donor gives a doped p - type semiconductor (p^+ semiconductor). In the first case the result is some electron charge carriers in the forbidden region (holes are minority carriers and current is mainly due to electrons), and in the second one is excess of hole charge carriers in the forbidden region (current is mainly due to holes).

[12] Also known as recombination centers.

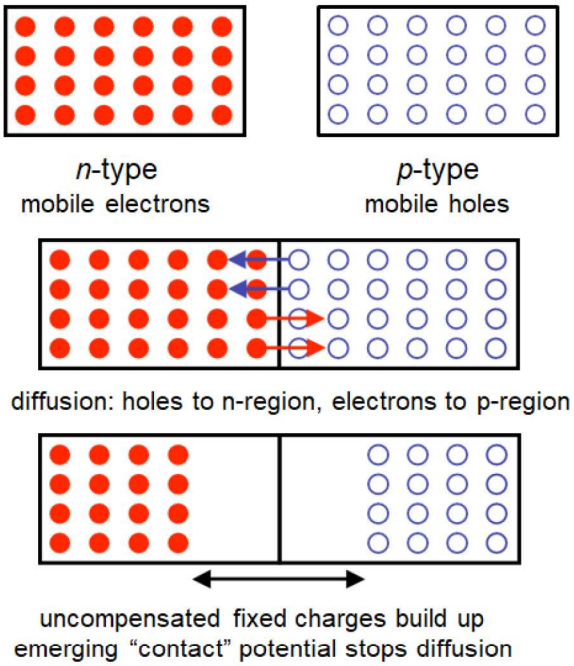

Figure 3.2.1: p - n junction [18]. Electrons move from n to p semiconductor and holes diffuse from p to n semiconductor. Depletion layer, that is free of charge carriers, is created at the boundary of the p - n junction. Fixed charges represent space charge and they are left behind.

p - type seminconductor in contact with n - type semiconductor gives p - n junction as shown in Figure 3.2.1. Electron - hole pairs are produced when incident radiation pass through p - n junction which is important part of semiconductor devices. Charge carriers need to be collected before they recombine. Migration of the electrons and holes under the influence of applied electric field generates a pulse of current, which is amplified. Forward bias and reverse bias are two ways of applying a voltage across the p - n junction. The first one is the direction of main current flow and the second one is the opposite direction i.e. little or no current. In the first case depletion zone becomes narrower, potential barrier becomes smaller and diffusion across junction becomes easier. This result is an increase of the current across junction. In the case of the reverse bias, the depletion zone becomes larger, potential barrier becomes higher and the current across the junction is very small leakage current.

Current pulses i.e. induced signals can be recorded with proper electronics and used to determine the energy, number or identity of incident particles. Energy level diagram of a p-type and n-type semiconductor and their configurations are illustrated in Figures 3.2.2. and 3.2.3,

respectively.

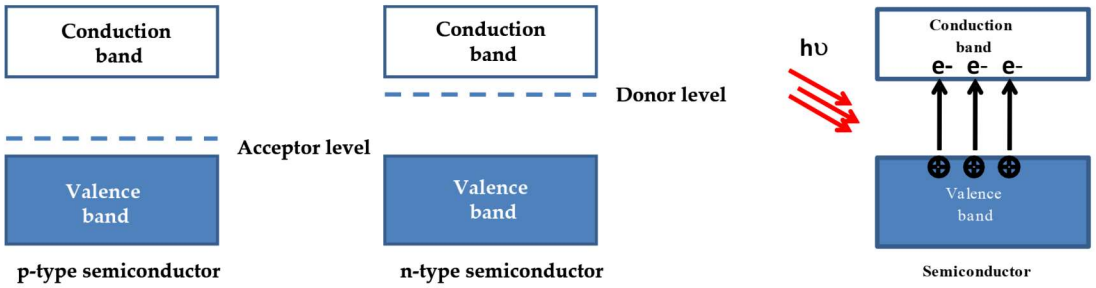

Figure 3.2.2: Energy band diagram of a p-type and n-type semiconductor [19]. By doping the semiconductor material, concentration of either holes or electrons is increased, which adds a new energy level in the band structure. When radiation passes through the detector material, equal numbers of electron - hole pairs are produced. The generated charges can be collected and recorded.

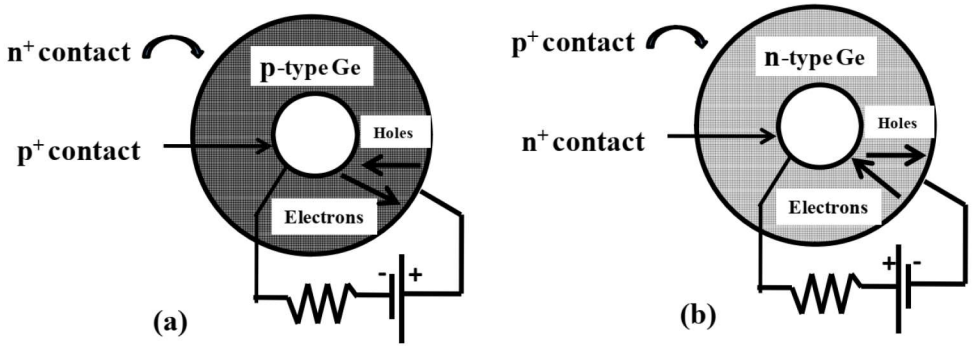

Figure 3.2.3: Structure of a (a) p-type and an (b) n-type closed-end co-axial detector [19].

Semiconductor materials have wide range of applications, from nuclear structure physics to the prevention of trafficking illegal nuclear materials. Different semiconductor materials are used for different purposes: silicon is primarly used to measure energy of charged particles and particle identification, whereas germanium is commonly used in γ - spectroscopy. Ge has relatively high atomic number ($Z = 32$) and a much higher photoelectric cross section [13] than silicon ($Z = 14$), which makes it more suitable for γ - detection. For this reason, it is more likely that γ - photon will be absorbed in germanium than in silicon and the intrinsic peak efficiency will be

[13]The cross section represents the probability that a certain interaction between an incident particle and a target will happen. It can be physically interpreted as an effective area of a target nucleus where a larger area indicates a larger probability of interaction.

significantly larger. Usually, the germanium crystal is sealed inside a cryostat. As a result of the small band gap (compared to Si), Ge need to be cooled down to reduce random formation of thermally generated charge carriers at the room temperature. Therefore, these type of detectors need to have cooling system in order to reduce background ("noise"). High energy resolution is one of the most important characteristics of semiconductor detectors. Other good properties of these detectors compared to the other ones are suitable size, good stopping power and relatively fast timing characteristics. *High - purity germanium* (HPGe) semiconductor detector is shown in Figure 3.2.4.

Figure 3.2.4: HPGe semiconductor detector [21].

4 Materials and Methods

Research presented in this thesis was performed at the Horia Hulubei Institute which is part of the Romanian Institute of Physics and Nuclear Engineering (IFIN-HH). 8 $LaBr_3$ detectors, 9 HPGe detectors and 2 silicon (Si) detectors were used in the experiment. $LaBr_3$ detectors are used because of their excellent coincidence time resolution and acceptable energy resolution, and are shown in Figure 4.0.1.

Figure 4.0.1: Photograph of encased "2 x 1.5" $LaBr_3$ detector with photomultiplier tube (PMT) attached used in the experiment [21].

Calibration of detectors was done beforehand with isotope ^{128}Eu and it is not described in this thesis. In the performed experiment ^{7}Li beam was accelerated to energy $E = 21$ MeV and impinged on a thick ^{96}Zr target. The target used in the experiment was $^{96}ZrO_2$ with a thickness of $300 \cdot 2$ μg/cm^2, which was backed with 10 mg/cm^2 Au. γ coincidence measurements were made with HPGe, Si and $LaBr_3$ scintilator γ detectors, but only data obtained from HPGe detectors were analyzed and presented in this work.

4.1 The goal of the experiment

Nuclei with atomic numbers close to 100 and with neutron numbers close to the sub - shell closure at 50 and 56 are in general not well - known at higher spins. These nuclei are close to the line of stability so they are not so readily populated by the fusion - evaporation reactions. Contrary, the largest yield of different channels populated by the transfer reactions belong to these nuclei which are placed in the vicinity of the projectile and target [22].

The performed reaction was $^{7}\mathrm{Li} + ^{96}\mathrm{Zr}$ and the main focus was to study the one - proton transfer reaction channel i.e. the $^{97}_{41}\mathrm{Nb}$ nucleus. To be specific, high - spin states in the $^{97}_{41}\mathrm{Nb}$ nucleus have been populated in fusion - evaporation reactions. Therefore, the initial goal of the experiment was to detect the γ - ray transitions from excited states populated in $^{97}_{41}\mathrm{Nb}$ with γ - detectors (HPGe and $LaBr_3$ scintilator γ - detectors) and to determine placement of the newly identified γ - rays in the decay scheme and their multipolarity [14]. In order to obtain that, the fusion reaction took place between projectile $^{7}\mathrm{Li}$ and the target $^{96}\mathrm{Zr}$:

$$^{7}_{3}\mathrm{Li} + ^{96}_{40}\mathrm{Zr} \longrightarrow ^{103}_{43}\mathrm{Tc}^{*}$$

However, after experiment was performed, the results have shown that observed γ - rays do not predominantly belong to $^{97}_{41}\mathrm{Nb}$ nucleus. This reaction produced a number of nuclei and the ones that have been identified so far and are a part of this thesis were $^{98}_{42}\mathrm{Mo}$, $^{100}_{42}\mathrm{Mo}$, $^{99}_{43}\mathrm{Tc}$ and $^{100}_{43}\mathrm{Tc}$. On top of that, γ transitions of the nucleus $^{99}_{43}\mathrm{Tc}$ and $^{100}_{43}\mathrm{Tc}$ prevailed among others.

[14] Only low - spin states i.e. spin lower than the $9/2^{+}$ ground state are known in the level scheme of ^{97}Nb.

5 Analysis and Results

Data analysis was done using the GaspWare software package. What we understand as "data" here, is the measured spectrum of the decay of interest, free of contaminants. In this experiment thick target was used, therefore all the outgoing particles of the reaction were stopped in the target. All used detectors gathered γ spectra of reaction products, but only results from HPGe detectors are presented here. Data obtained from other detectors were not analyzed since it is beyond the scope of this thesis. Initial γ spectrum of all the recorded γ transitions that follow the $^{7}\mathrm{Li} + {}^{96}\mathrm{Zr}$ reaction is shown in Figure 5.0.1. Our goal is to determine which γ transition belongs to which nucleus i.e. to obtain γ spectrum of each nucleus created in the reaction. We observed that most γ transitions in the spectrum shown in Figure 5.0.1. belong to ^{99}Tc nucleus, which has relatively long half-life (approximately 211 years [23]). Therefore, it makes it harder to identify γ transitions of other nuclei created in the reaction.

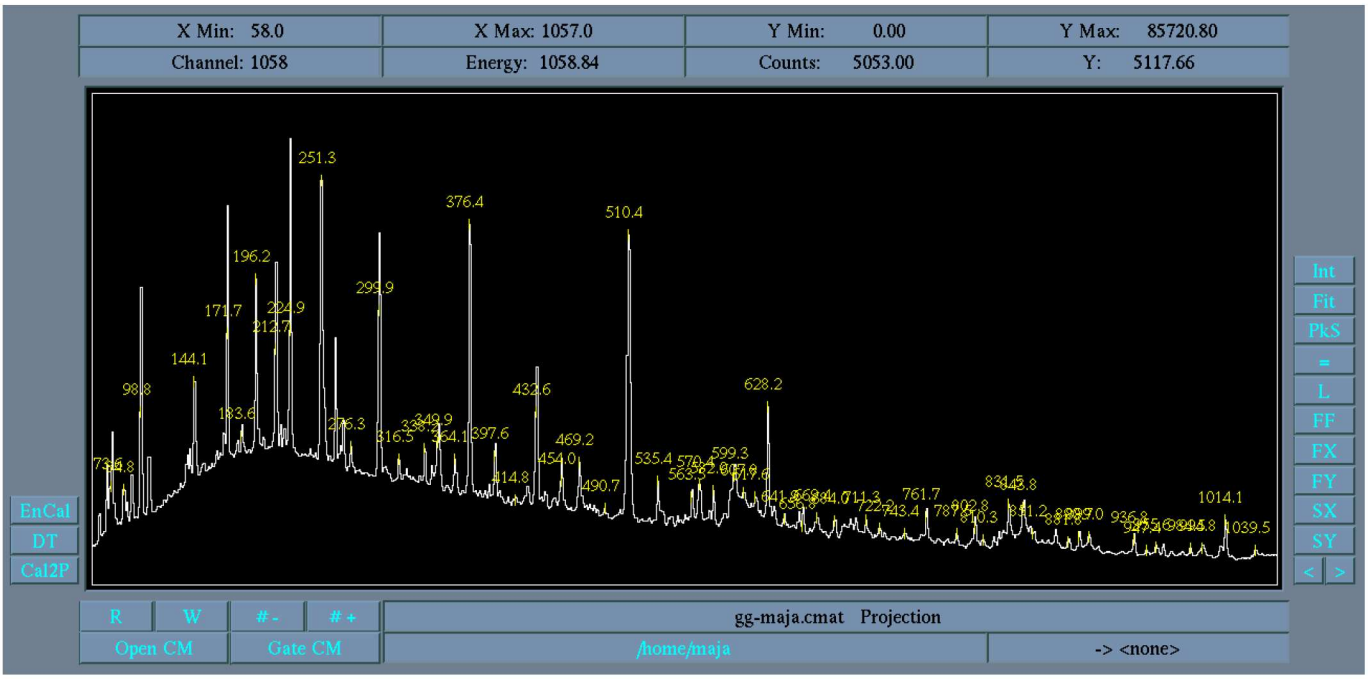

Figure 5.0.1: γ spectrum in XTRACKN program. Initial spectrum has channels from 0 to 4089 keV.

Different nuclei may be identified by their characteristic γ - ray transitions. The use of multiple HPGe detectors enabled coincidence γ - spectrometry, i.e. coincident (near simultaneous) signals coming from cascade of γ - decays can be extracted. Figure 5.0.1. shows γ - γ coincidence

spectrum, i.e. only γ - rays that are detected in coincidence with at least one other γ - ray are presented in the spectrum.

By putting gates (conditions on the energy range) on different energy peaks we can narrow the spectrum to the γ - rays that are in coincidence with the specific γ - ray. That way, we can, from the initial γ spectrum (of all the detected nuclei) extract spectra from individual nuclei, only by putting gates on several γ peaks that are previously known for that specific nucleus.

In order to extract the γ spectrum of certain isotope, XTRACKN program was used. XTRACKN program is part of the GaspWare software package and is designed for analysis of γ spectra. Unfortunately, since most of the γ - energies in the original spectrum come from ^{99}Tc nucleus, and it has similar energies as γ - rays from neighbouring isotopes (which results in very high background noise), we couldn't obtain clear γ spectra of individual nuclei in the way described above, but we did following procedure instead.

1. $\gamma - \gamma$ spectrum is based on time coincidences and by putting a gate on at least one γ - ray from original spectrum, only those γ - rays that are in coincidence with gated one will appear in the spectrum. The γ - ray peak for which is previously known that it belongs to the nucleus of interest (e.g. ^{100}Tc) is tagged taking 2 or 3 channels on each side of the center of peak (Figure 5.0.2.). γ - rays that are in coincidence with the tagged one are visible in the upper frame in Figure 5.0.3. The name of the obtained spectrum is *center*.

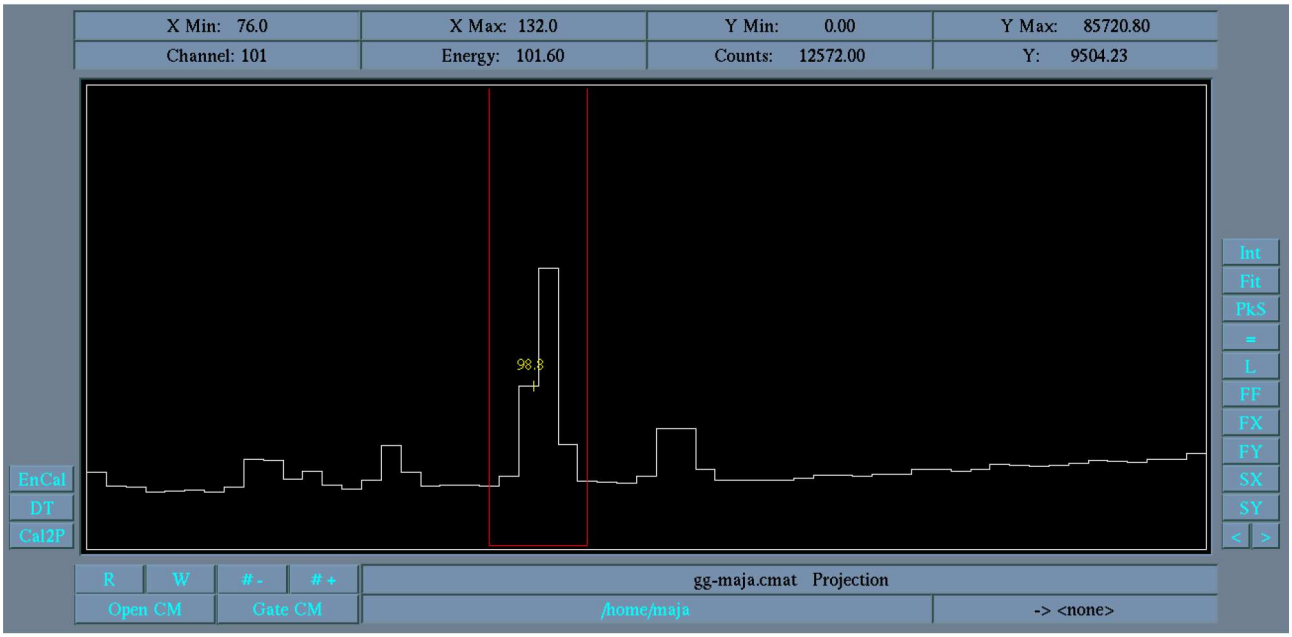

Figure 5.0.2: Gated γ - ray transition 99 keV.

2. Following this, and for the purpose to find the background noise, gates (two dimensional conditions on the energy) were put on both sides of γ - ray peak of interest (as close to the peaks as possible), taking the same number of channels as it is in the gate of interest. Coincident γ - rays obtained this way are presented in center and lower frames in Figure 5.0.3. The spectra are named $left$ and $right$. We notice that the spectrum contains some other γ-rays besides these coming from ^{100}Tc (e.g. 196 keV and 300 keV).

3. Two γ - ray peaks that don't belong to the decay scheme of the isotope of interest were gated in all the three spectra in Figure 5.0.3. and the number of events (i.e. the area below the peak) in those γ - rays are denoted $center\_1$, $center\_2$, $left\_1$, $left\_2$, $right\_1$ and $right\_2$.

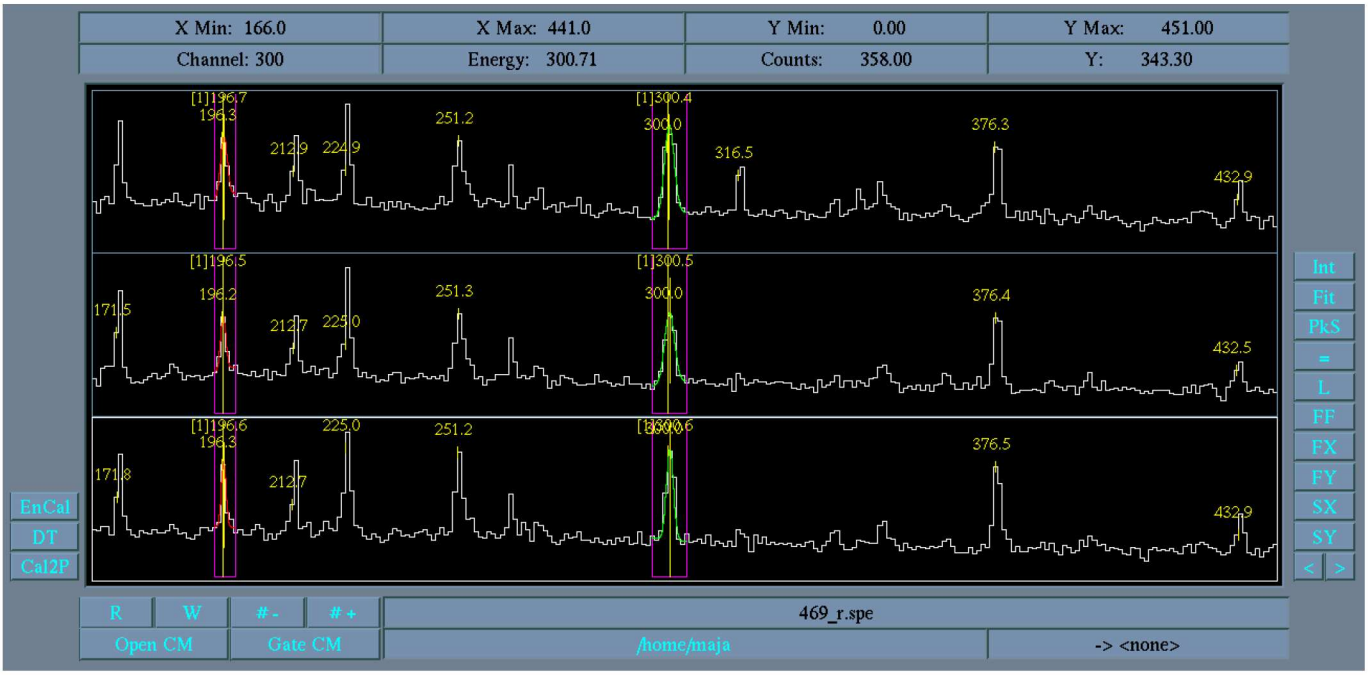

Figure 5.0.3: Gates on the γ - ray peaks which don't belong to the specific isotope of interest. Center, left and right spectrum are shown in top, middle and bottom frame, respectively.

To remove background from the ^{100}Tc spectrum, parameters a and b were found by solving following equations:

$$center\_1 - right\_1 \cdot b - left\_1 \cdot a = 0$$

$$center\_2 - right\_2 \cdot b - left\_2 \cdot a = 0$$

These parameters were used to clean the initial spectrum by using program SADD. Firstly, spectrum *right* is input with INPUT command and is multiplied by parameter $-b$ channel by channel. After multiplying the matrix spectrum, a command ADD is used, which creates new matrix by summing the matrices $-b \cdot right$ and $center$, channel by channel i.e. one subtracts matrix $-b \cdot right$ from $center$. New matrix is saved under the name *res*. The same procedure is repeated with spectrum $left$, which is multiplied by parameter $-a$. Finally, this matrix is added to the matrix *res* in order to gain the final spectrum which is written under the name $clean$. This process is shown in Figure 5.0.4.

If the results don't fit well to the data from NNDC [15], which provides experimental information on nuclear structure and nuclear reactions, the procedure has to be repeated by selecting the different γ - ray peaks and therefore changing the parameters a and b. After cleaned γ spectrum for specific isotope is obtained, we have used XMGLS program to construct the level scheme.

```
maja@maja-VirtualBox:~$ sadd


 SADD  VAX/VMS   V2.1   2-FEB-1989
 INPUT           file_name|L:8
 OUTPUT          file_name|L:8
 ADD-MULT-DIV    file_name|L:8
 SADD> input right.spe|L:4
 INPUT     right.spe|L:4
 SADD> multfactor -0.5131
 MULT   Factor: -0.5131000       [     0  --  4095  ]
 SADD> add center.spe|L:4
 ADD    Factor:   1.000000         center.spe|L:4
 SADD> output res.spe|L:4
 OUT    res.spe|L:4
 SADD> input left.spe|L:4
 INPUT     left.spe|L:4
 SADD> multfactor -0.2886
 MULT   Factor: -0.2886000       [     0  --  4095  ]
 SADD> add res.spe|L:4
 ADD    Factor:   1.000000         res.spe|L:4
 SADD> output clean.spe|L:4
 OUT    clean.spe|L:4
 SADD>
```

Figure 5.0.4: Process of cleaning original spectrum in SADD program

[15] National Nuclear Data Center

6 Results and Discussion

Initial γ spectrum is shown in Figure 5.0.1. Most γ transitions observed in the $^{7}\mathrm{Li} + {}^{96}\mathrm{Zr}$ reaction belong to the nucleus $^{99}_{43}\mathrm{Tc}$ and $^{100}_{43}\mathrm{Tc}$ whose γ spectra (cleaned from background noise, as explained in the previous section) are shown in Figures 6.0.1. and 6.0.2.

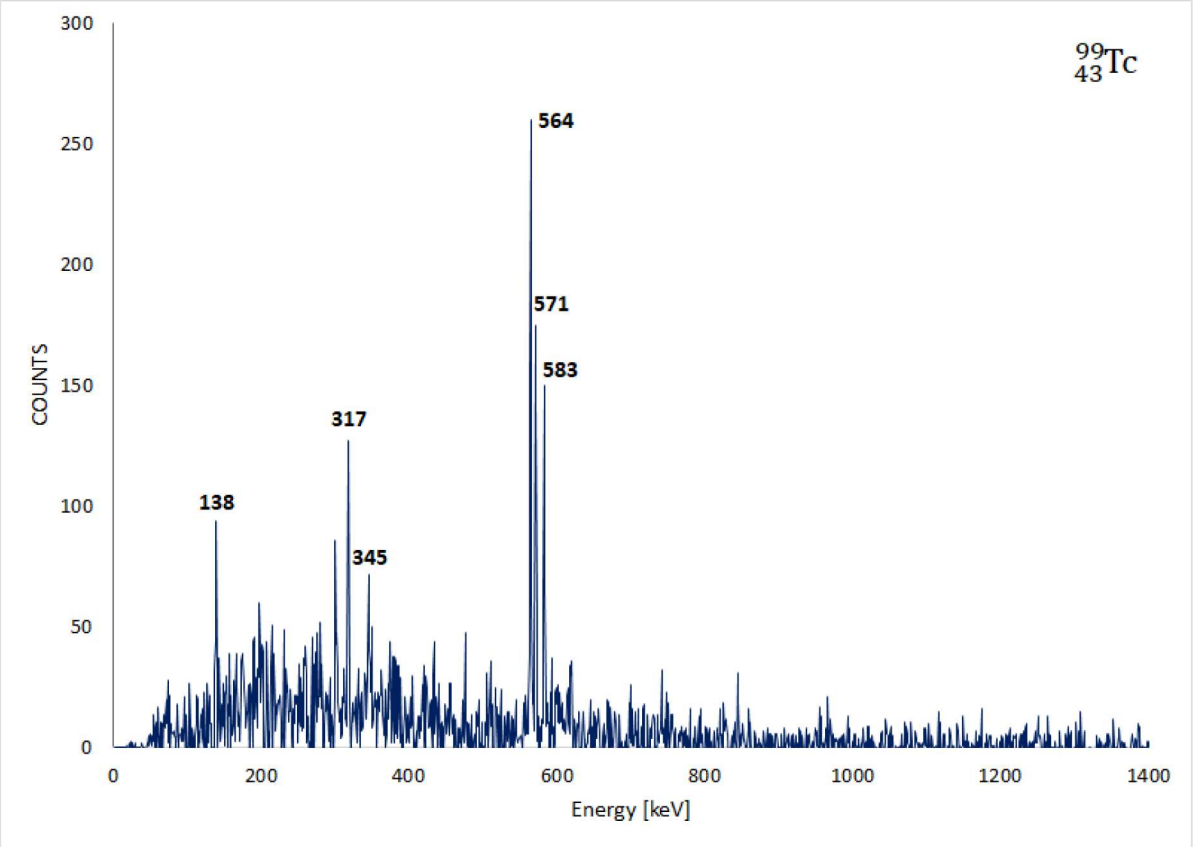

Figure 6.0.1: The γ - ray spectrum obtained after putting a gate on the 470 keV γ - transition in ^{99}Tc.

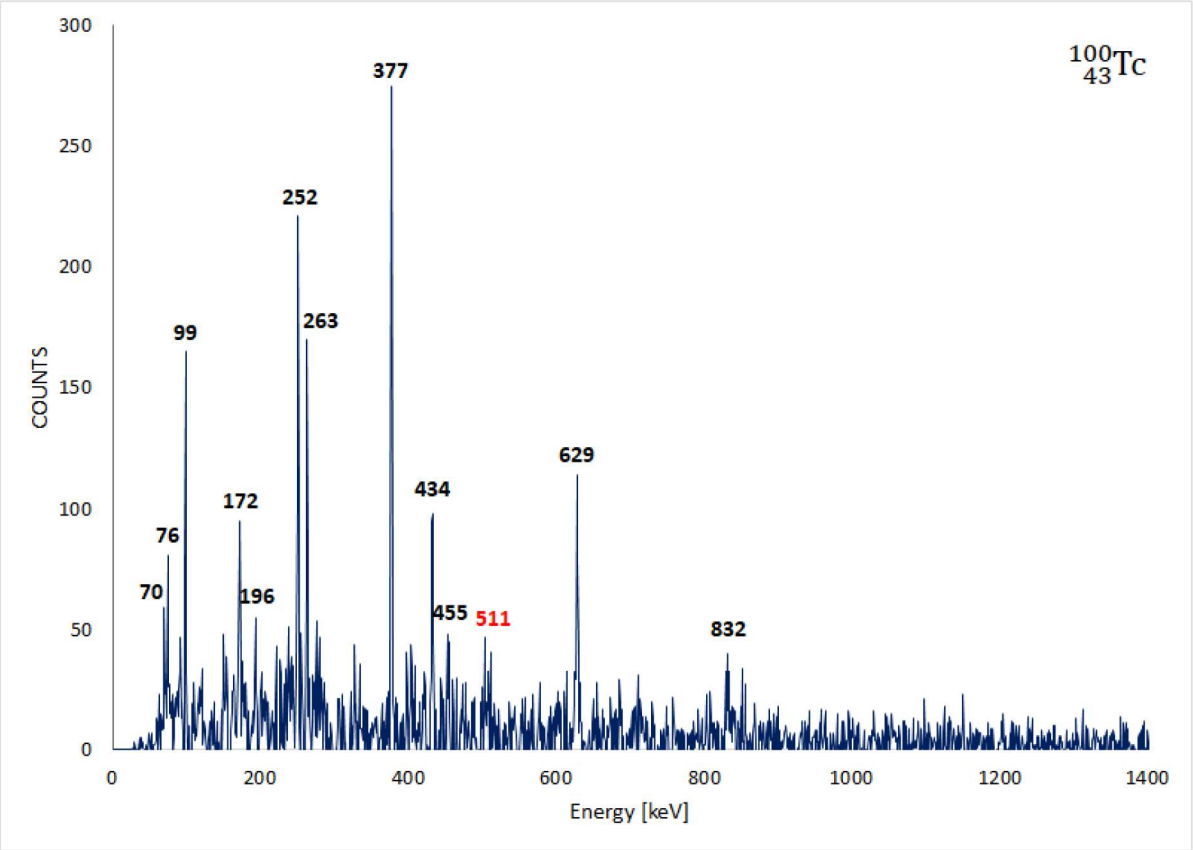

Figure 6.0.2: The γ - ray spectrum of ^{100}Tc obtained by gating the 225 keV in the ^{7}Li + ^{96}Zr reaction.

This result is expected because the nucleus created in fusion reaction is excited nucleus ^{103}Tc. Nuclei ^{99}Tc and ^{100}Tc are obtained by fusion followed by evaporation of neutrons:

$$^{7}_{3}\mathrm{Li} + ^{96}_{40}\mathrm{Zr} \longrightarrow ^{103}_{43}\mathrm{Tc}^{*} \longrightarrow 4\,^{1}_{0}\mathrm{n} + ^{99}_{43}\mathrm{Tc}$$

$$^{7}_{3}\mathrm{Li} + ^{96}_{40}\mathrm{Zr} \longrightarrow ^{103}_{43}\mathrm{Tc}^{*} \longrightarrow 3\,^{1}_{0}\mathrm{n} + ^{100}_{43}\mathrm{Tc}$$

γ - rays energies from the yrast levels of ^{99}Tc observed in the ^{7}Li + ^{96}Zr reaction were: 138, 317, 345, 470, 564, 571 and 583 keV and are shown as the level scheme in Figure 6.0.3. γ transition 143 keV from the 143 keV level to 0 keV level wasn't seen. This is because it predominantly decays by internal conversion. Moreover, 455 keV which belongs to the 2785 keV $\longrightarrow$ 2330 keV transition wasn't observed, probably because it was assigned to ^{100}Tc and removed during the spectrum extraction. Energies, spins and parities of levels are as in NNDC [23].

The high-spin states of ^{99}Tc were previously observed in the fusion-evaporation reaction ^{96}Zr(^{7}Li, 4n) [24] and ^{96}Zr(^{6}Li, 3n) [25, 26]. Compared to the lighter isotopes of technetium, the cascade of ^{99}Tc doesn't only consist of E2-transitions. Moreover, there is an increase of aligned angular momentum at energy $\hbar\omega \sim 0.26$ MeV with much stronger intraband M1 transitions [24]. One explanation is that the structure above 2646.5-keV ($19/2^-$) level is based on a similar configuration as the π $g_{9/2}\times$ ($d_{5/2}$ $h_{11/2}$) configuration of the isotone ^{101}Rh. According to the Reference [24], another possibility includes the mixing of the $p_{1/2}$ $1/2^-$ Nilsson orbital with the $f_{5/2}$ $3/2^-$ orbital at medium spins. Transitions between the $3/2^-$ and $1/2^-$ bands would be much larger than the pure intraband M1 transitions because they are spin-flip transitions [24]. Third scenario involves shape change. The ^{99}Tc nucleus belongs to the transitional region and is a good candidate for triaxiality (axial deformation). Strong M1 transitions turning to strong E2 transitions at low spins is characteristic of a shape change from spherical to deformed nuclei [24].

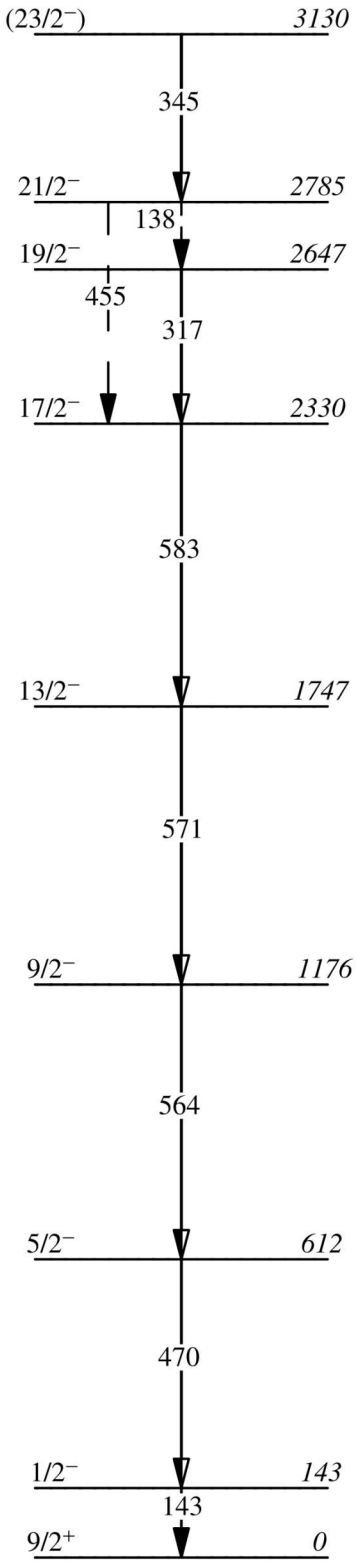

Figure 6.0.3: The energy level scheme of ^{99}Tc deducted from the experiment.

The energy level scheme of isotope ^{100}Tc is shown in Figure 6.0.4. γ - rays from the yrast levels of ^{100}Tc observed in the experiment were: 70, 76, 99, 172, 252, 377, 434, 455 and 629 keV. γ - ray line at 511 keV doesn't belong to the level scheme of ^{100}Tc and it is a result of electron - positron annihilation. γ - ray of 398 keV was marked with the dashed line because it wasn't seen in the resulting γ spectrum. The reason may be lower branching ratio $I(\gamma) = 67\%$ [23]). γ transition 831 keV ($I(\gamma) = 100\%$ [23]) from 2238 keV to 1407 keV wasn't strongly seen in the cleaned spectrum since 834 keV was assigned to ^{98}Mo and it was probably removed during the extraction. In addition, γ - ray transitions 28, 43 and 64 keV weren't found which is associated with lower efficiency of HPGe detector for low-energy γ - rays. γ - ray 196 keV is newly identified transition and it has yet to be assigned to a certain γ transition.

Although there are less γ transitions observed in our experiment, these results are in agreement with the earlier measurements [27]. In the present experiment we observed the yrast states up to 14^-. The negative parity band may arise from the $h_{11/2}$ neutron coupled to the $g_{9/2}$ proton as suggested in prior study [27]. Previous work on ^{100}Tc has determined excited states up to spin 16 in the yrast negative-parity band. It was observed in fusion-evaporation reaction ^{96}Zr(^{7}Li, 3n) [27], and valence particles at these energies are primarily $g_{9/2}$, $p_{1/2}$ for proton and $d_{5/2}$, $g_{7/2}$ and $h_{11/2}$ for neutron.

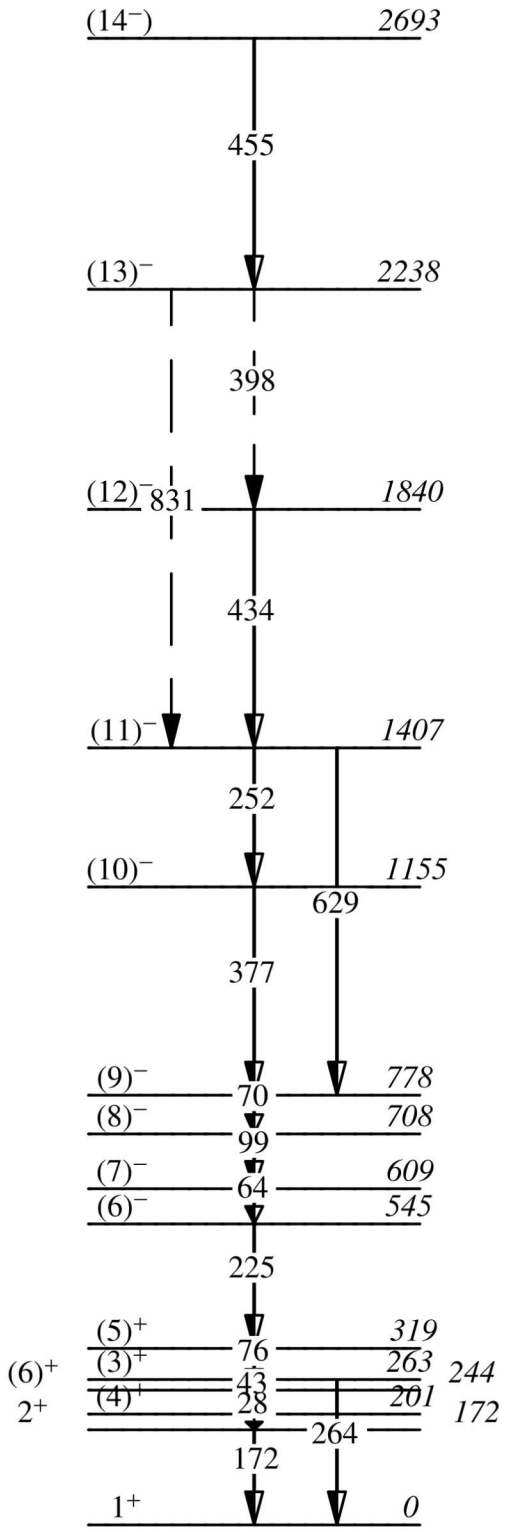

Figure 6.0.4: The energy level scheme of isotope ^{100}Tc obtained from the present measurements.

The γ - ray spectrum of isotope ^{98}Mo was obtained by gating on the 787 keV and is presented in Figure 6.0.6. The cascade of four transitions has been observed and assigned to the positive - parity yrast band built on the 0^+ ground state. Therefore, E_γ = 227 keV as the (6, 7, 8) $\longrightarrow 6^+$, E_γ = 834 keV as the $6^+ \longrightarrow 4^+$, E_γ = 723 keV as the $4^+ \longrightarrow 2^+$, E_γ = 787 keV as the $2^+ \longrightarrow 0^+$ transition.

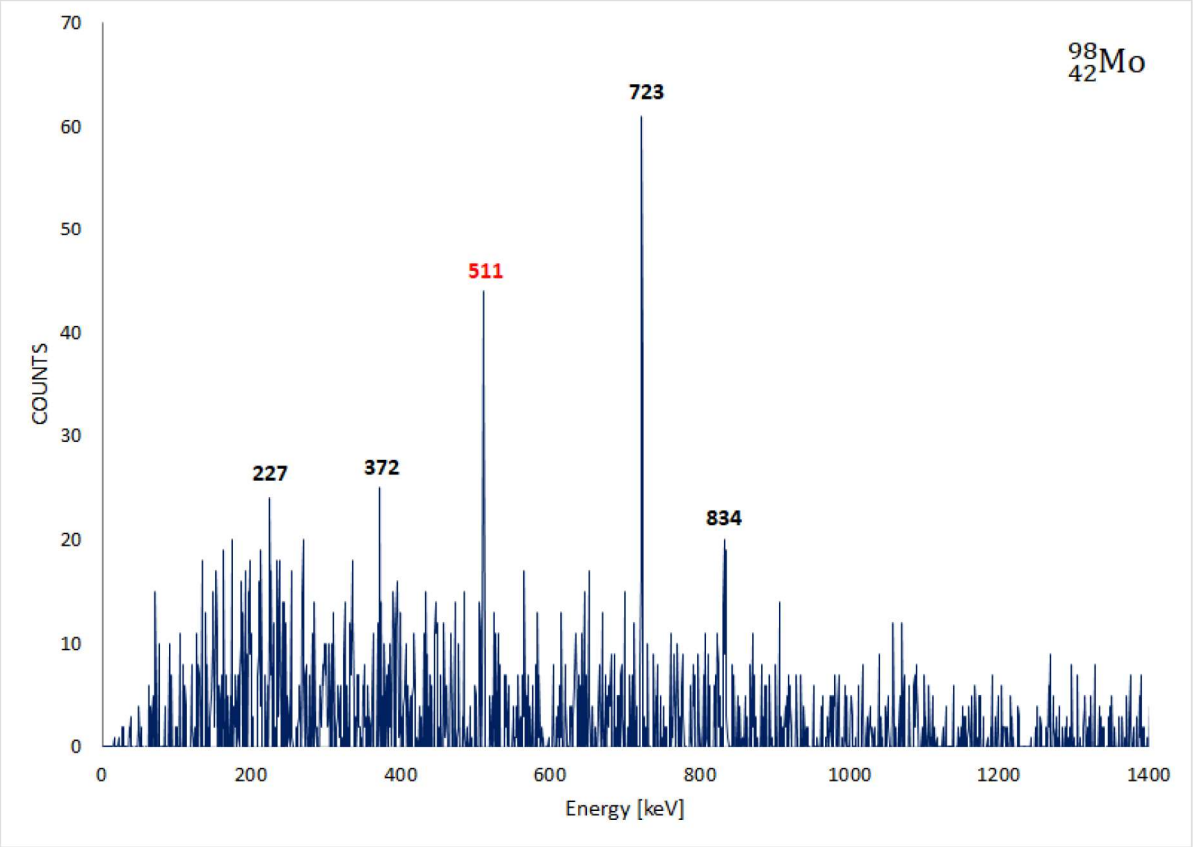

Figure 6.0.5: The γ - ray spectrum of ^{98}Mo obtained by gating on the 787 keV in the ^{7}Li + ^{96}Zr reaction.

Transitions observed in the experiment are shown as the level scheme in Figure 6.0.6. Obtained level scheme of ^{98}Mo is in good correspondence with earlier study [28]. It is interesting to notice that the highest observed state in ^{98}Mo was previously observed only in fusion-evaporation reaction ^{96}Zr(α, 2nγ). According to the Reference [28], the lowest 6^+ states are probably predominantly $d_{5/2}$ and $g_{7/2}$ excitations for neutron.

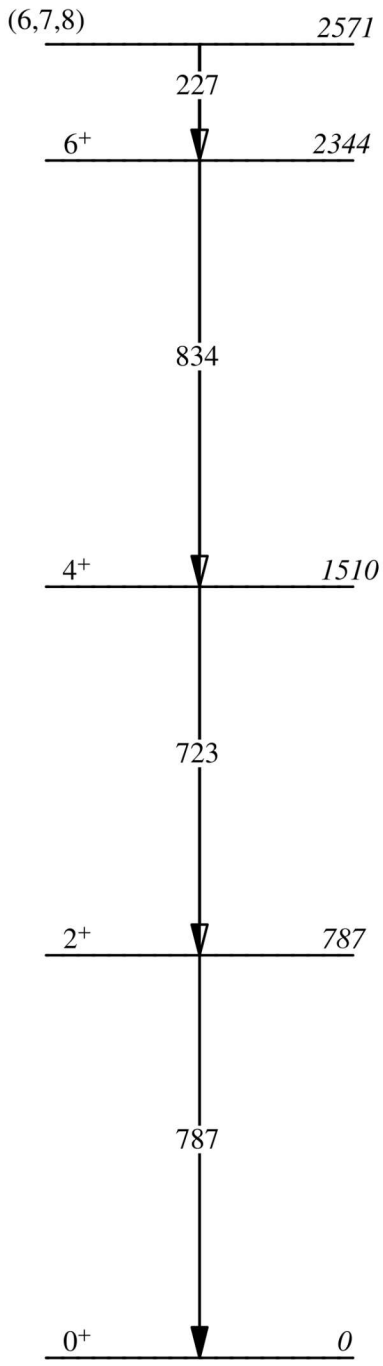

Figure 6.0.6: Energy level scheme of isotope ^{98}Mo.

The energy level scheme of isotope ^{100}Mo was created based on the obtained γ spectrum of ^{100}Mo (Figure 6.0.7.). The higher - spin yrast states were established up to 10^+. γ - rays from the yrast levels of ^{100}Mo observed in the experiment were: 740, 711, 780 and 600 keV. The gate was set on γ - ray 536 keV. The sequence of γ - rays 740 keV as the $10^+ \longrightarrow 8^+$, 780 keV as the $8^+ \longrightarrow 6^+$, 711 keV as the $6^+ \longrightarrow 4^+$, 600 keV as the $4^+ \longrightarrow 2^+$ and 536 keV as the $2^+ \longrightarrow 0^+$ transition has been recognized for the decay. All these transitions are shown in Figures 6.0.7. and 6.0.8.

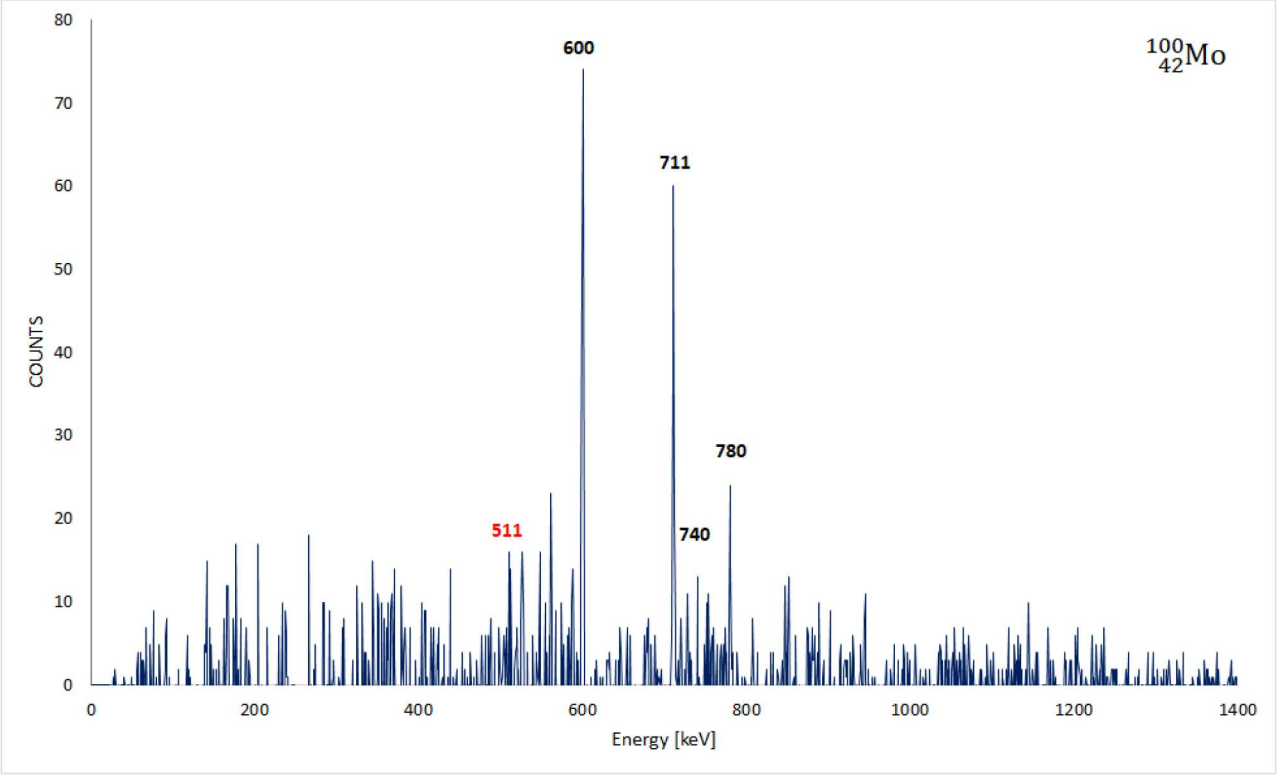

Figure 6.0.7: The γ - ray spectrum of ^{100}Mo obtained by gating on the 536 keV in the ^{7}Li + ^{96}Zr reaction.

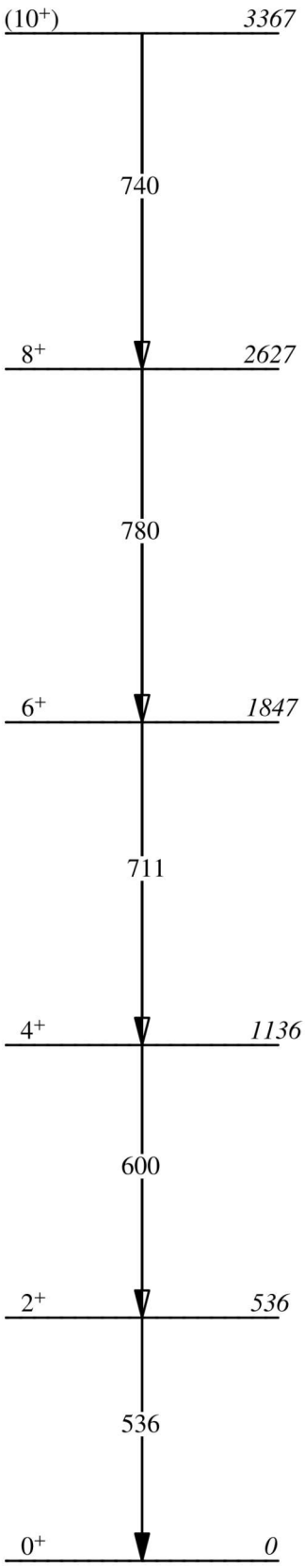

Figure 6.0.8: Energy level scheme of isotope ^{100}Mo.

7 Conclusion

γ - ray spectroscopy is a basic tool for studying neutron - rich nuclei by using fusion-evaporation reactions. These reactions have been studied for the $^{7}\mathrm{Li} + {}^{96}\mathrm{Zr}$ system. The experiment was performed using 8 $LaBr_3$, 9 HPGe detectors and 2 Si detectors. The dominant contribution to the obtained γ - ray spectrum arises from the ^{99}Tc nucleus. In the $^{7}\mathrm{Li} + {}^{96}\mathrm{Zr}$ fusion-evaporation reactions, outgoing particles with the atomic number $Z = \{42, 43\}$ and mass number $A = \{98 - 100\}$ were identified. The γ spectrum of each nucleus is presented along with recognized γ - rays. Based on these spectra, level schemes were constructed. In total, 26 γ - ray transitions have been determined from analysing data of γ - γ spectrum. These γ - ray transitions have been assigned to the isotopes: ^{99}Tc, ^{100}Tc, ^{98}Mo and ^{100}Mo. New γ - ray transition 196 keV that can be exclusively assigned to the ^{100}Tc isotope has been identified. Obtained energy level schemes were compared with previous studies of these nuclei and it can be concluded that they are in agreement with the cited ones.

8 References

[1] Nuclear Physics. // Fundamentals of Physics Extended - 9th Edition / Halliday, D.; Resnick, R.; Walker, J.; Cleveland: John Wiley and Sons, 2011., 1165-1195.

[2] Wikipedia. // https://en.wikipedia.org/wiki/Magic_number_(physics) [18.04.2019.]

[3] Casten, R. Nuclear Structure From A Simple Perspective : Introduction. New York : Oxford University Press, 1990.

[4] Nuclear Reactions and Their Applications. // Chemistry - The Molecular Nature of Matter and Change / Silberberg, M. S.; Amateis, G. P.; New York: McGeaw - Hi Higher Education, 2009., 1053-1090.

[5] Mayer, M. G.; Jensen, J. Elementary Theory of Nuclear Shell Structure. New York : John Wiley and Sons, 1995.

[6] Radioactive Decay and the Origin of Gamma and X-Radiation. // Practical Gamma - ray Spectrometry - 2nd Edition / Gilmore, G. R.; Warrington: John Wiley and Sons, 2008., 1-24.

[7] National Research Council. Nuclear Physics - Exploring the Heart of Matter : Science Questions. Washington, D.C. : National Academies Press, 2013.

[8] Austern, N. Direct Nuclear Reaction Theories. New York : John Wiley and Sons, 1970.

[9] Henning, G. Stability of Transfermium Elements at High Spin: Measuring the Fission Barrier of 254No. Universite Paris Sud - Paris XI, 2012.

[10] Neyens, G. Nuclear magnetic and quadrupole moments for nuclear structure research of exotic nuclei. // Reports on Progress in Physics. 66, 2013, 633-689.

[11] Radiation Interactions. // Radiation Detection and Measurement / Knoll, G. F.; New York: John Wiley and Sons, 2000, 29-57.

[12] Cherry, S. R.; Sorenson, J. A.; Phelps, M. E. Physics in Nuclear Medicine. Philadelphia : Saunders, 2012.

[13] Scintillation Detector Principles. // Radiation Detection and Measurement - 3rd Edition / Knoll, G. F.: John Wiley and Sons, 1999, 219-247.

[14] Chemistry LibreTexts. // https://chem.libretexts.org/ [18.04.2019.]

[15] Wikipedia. // https://en.wikipedia.org/wiki/Scintillation_counter [26.02.2019.]

[16] Ortec page. // https://www.ortec-online.com/products/radiation-detectors/scintillation-detectors/scintillation-detector-types/lanthanum-bromide-detectors [26.02.2019.]

[17] Semiconductor Diode Detectors. // Radiation Detection and Measurement - 3rd Edition / Knoll, G. F.: John Wiley and Sons, 1999, 353-405.

[18] Brom, J. M. Detector Technologies - Semiconductors. // https://slideplayer.com/slide/8960436/ [26.02.2019.]

[19] Shodhganga: Experimental and theoretical techniques // http://shodhganga.inflibnet.ac.in/bitstream/10603/4710/11/11_chapter%202.pdf [18.04.2019.]

[20] Ortec page. // https://www.ortec-online.com/products/radiation-detectors/germanium-hpge-radiation-detectors [26.02.2019.]

[21] Regan, P. H. et al. Precision Lifetime Measurements Using $LaBr_3$ Detectors With Stable and Radioactive Beams. EPJ Web of Conferences 63, 2013. URL: url-http://dx.doi.org/10.1051/epjconf/20136301008 [18.04.2019.]

[22] Szilner, S. et al. High-spin states in the ^{97}Nb nucleus populated in the ^{40}Ca+^{96}Zr multinucleon transfer reaction by PRISMA+CLARA, 2006. URL: http://clara.pd.infn.it/reports/2006/025_A_54_A049.pdf [18.04.2019.]

[23] National Nuclear Data Center. // https://www.nndc.bnl.gov/ [04.05.2019.]

[24] Xiao, Z.G. et. al. Collective band structures in the ^{99}Tc nucleus. // Physical Review C. 91(5), 2015.

[25] Zell, K.O. et al. High-Spin States in $^{99}Tc^{*}$. // Z. Pys. A - Atoms and Nuclei. 316, 1984, 351-359.

[26] Kajrys, G. et al. High spin states in ^{99}Tc. // Physical Review C. 31(2), 1985, 409-415.

[27] Bizzeti-Sona, A.M. ; Blasi, P. ; Stefanini, A.A. ; Maino, G. ; Ventura, A. Yrast States in the Doubly-Odd Nucleus ^{100}Tc. // Z.Phys. A. 352, 1995, 247-255.

[28] Lederer, C.M. et al. In-beam gamma-ray spectroscopy of even Mo and Ru isotopes. // Nuclear Physics A. 169, 1971, 449-488.

9 Curriculum Vitae

Irena Lukanović was born on the 4th of December 1994 in Vinkovci (Croatia). She grew up in a family which consists of 5 members: parents Ivo and Manda, and two older sisters, Marina and Ivana. In 2013 she finished secondary school in Vinkovci and got admitted to the University of J.J. Strossmayer in Osijek. From 2013 till 2016 she obtained her Bachelor degree in physics and continued her master studies at the J. J. Strossmayer University of Osijek, Department of Physics. From July 2016 till September 2016 she did an IAESTE Internship program in Austria, at the Erich Schmid Institute of Materials Science. In 2017 she finished a student internship in Warsaw at the Institute of High Pressure Physics (Poland). During her studies she participated in the 11th Symposium of the Croatian radiation protection association held in Osijek (Croatia) in 2017 and in the 10th and 11th Scientific Meeting of Croatian Physical Society held in Baška in 2017 and in Beli Manastir in 2018 (Croatia). She received the Rector's Award for her outstanding academic achievements in year 2014/2015, 2015/2016 and 2016/2017.

She has played handball in the club ŽRK Vinkovci for more than 10 years. In her free time she likes to play chess with her father.